

**University of Reading**  
**School of Mathematical and Physical Sciences**

**Computation and Analysis of Baroclinic Rossby  
Wave Rays in the Atlantic and Pacific Oceans**

**James Barlow**

August 2010

---

This dissertation is a joint MSc in the Departments of Mathematics and Meteorology and is  
submitted in partial fulfilment of the requirements for the degree of Master of Science

## Acknowledgments

I would firstly like to give a special thanks to my supervisor, Dr. Remi Tailleux, who's help and enthusiasm made this project so enjoyable. I would also like to thank the National Environmental Research Council (NERC) whose generous funding allowed me to take part in this course. Finally I would like to thank my family and friends for keeping me in high spirits throughout this very challenging year.

## Declaration

I confirm that this is my own work and the use of all materials from other sources have been properly and fully acknowledged.

Signed..... Date.....

## Abstract

In this study, wave dispersion is investigated as a possible mechanism in limiting the western extent of the offshore propagation of baroclinic Rossby waves, which has recently been observed in Topex/Poseidon satellite altimeter data. The technique of ray tracing is used, and a model developed, to calculate Rossby wave ray trajectories initially in the framework of Quasi-Geostrophic theory on the equatorial  $\beta$ -plane, and then in spherical polar coordinates. The model is also extended to account for the coastal geometry of the Atlantic and Pacific Ocean basins, and an analytical function is derived such that a gravity-wave phase speed distribution representative of either ocean basin is used to determine the Rossby radius of deformation. From the resulting ray propagation pattern, an attempt is made to determine the location of the theoretical coastic lines, westward of which, Rossby waves excited at the eastern boundary are expected to decay exponentially. A comparison is then made between the modelled caustics and sea surface height (SSH) data from the French CLIPPER model. Despite some data processing issues, the results indicate that the pattern of SSH variability in the South Atlantic Ocean is indicative of the shape of the coastics predicted by the model. This suggests that dispersion rather than dissipation is a likely mechanism to account for the observed westward decay of boundary-driven Rossby waves, and that Rossby waves observed in the western part of the ocean basin are likely to have been generated by a different mechanism.

# Contents

<b>1</b>	<b>Introduction</b>	<b>1</b>
1.1	Theory . . . . .	6
1.1.1	A Note On WKB Theory . . . . .	6
1.1.2	Dispersion Relationship . . . . .	6
1.1.3	Ray Equations . . . . .	9
1.1.4	Analytical Solution . . . . .	10
<b>2</b>	<b>Model Derivation and Results</b>	<b>14</b>
2.1	Cartesian Coordinates . . . . .	14
2.1.1	Ray Equations . . . . .	14
2.1.2	Autonomous Equations . . . . .	15
2.1.3	Fixed $k_x$ Solution . . . . .	16
2.1.4	Fixed $\omega$ Solution . . . . .	18
2.1.5	Critical Latitude . . . . .	19
2.1.6	Realistic Coastlines . . . . .	21
2.1.7	Variable Meridional Wavenumber . . . . .	23
2.1.8	Variable $c_0$ . . . . .	28
2.2	Spherical Polar Coordinates . . . . .	35
2.2.1	Dispersion Relationship . . . . .	35
2.2.2	Ray Equations . . . . .	35
2.2.3	Autonomous Equations . . . . .	36
2.2.4	Fixed $\omega$ Solution . . . . .	37
2.2.5	Critical Latitude . . . . .	37
2.2.6	Realistic Coastlines . . . . .	40
2.2.7	Variable Meridional Wavenumber . . . . .	41
2.2.8	Variable $c_0$ . . . . .	43
2.3	Caustics . . . . .	45
<b>3</b>	<b>Analysis of Model Output</b>	<b>48</b>

<b>4</b>	<b>Conclusions and Further Work</b>	<b>52</b>
4.1	Summary . . . . .	52
4.2	Further Work . . . . .	54
4.2.1	Model Improvements . . . . .	54
4.2.2	Ocean Data Analysis . . . . .	56
<b>5</b>	<b>Appendix 1</b>	<b>58</b>
5.1	Variable $c_0$ Equation - Cartesian Coordinates . . . . .	58
5.2	Variable $c_0$ Equation - Spherical Polar Coordinates . . . . .	59
<b>6</b>	<b>References</b>	<b>61</b>

# List of Figures

1.1	White lines identify a westward propagating, $\beta$ -refracted Rossby wave trough where the two diagrams are separated by a time period of 3 months. The image is taken from Chelton and Schlax (1996) and is based on T/P data. . . . .	2
1.2	Correlation coefficients between SSH variability and boundary-driven Rossby waves having had wind driven anomalies removed from the data (Fu and Qiu, 2002) . . . . .	3
1.3	A wave envelope. . . . .	4
1.4	A simple example of a ray propagation pattern from a straight, north-south orientated boundary for semi-annual frequency Rossby waves (Schopf et al. 1981). . . . .	5
1.5	Analytic solution from equations (1.41) and (1.42) for semi-annual frequency Rossby waves. . . . .	12
2.1	Ray paths from a straight boundary with a fixed $k_x$ . . . . .	17
2.2	Comparison of analytical (red) and numerical (black) solution for semi-annual frequency oceanic Rossby waves. . . . .	19
2.3	Fixed $\omega$ solution focused on the northern hemisphere. The red dashed line represents the critical latitude $y_c$ north of which no waves propagate from the eastern boundary. . . . .	20
2.4	Ray solutions for (a) Atlantic and (b) Pacific coastline geometry under the assumption of a zero meridional wavenumber along the boundary and constant $c_0$ . . . . .	22
2.5	Rays from a sloping eastern boundary. . . . .	24
2.6	Rays propagating on a local scale from the south-eastern Pacific coastline. . . . .	26
2.7	Ray paths with variable meridional wavenumber at the boundary for (a) Atlantic Ocean and (b) Pacific Ocean. Red circles indicate latitudes beyond the critical latitude or at which no Rossby wave propagation occurs due to the angle of the coastline. . . . .	27

2.8	(a) The global zonally averaged first order baroclinic mode gravity-wave phase speed obtained by Chelton et al. (1998). (b) The latitudinal variation in gravity-wave phase speed provided by the derived function specified by equation (2.37). . . . .	29
2.9	A comparison of the zonally averaged phase speed for (a) the Atlantic Ocean and (b) the Pacific Ocean, with the analytical function using the specified parameters for each respective ocean basin. . . . .	29
2.10	Meridionally averaged phase speeds for the Atlantic and Pacific oceans where $0^\circ$ longitude represents the eastern coastline. . . . .	30
2.11	Error between the observed phase speeds and (a) constant $c_0$ (b) analytic function $c_0(y)$ in the Atlantic Ocean. Phase speed errors $<0.3\text{ms}^{-1}$ are shown in yellow. . . . .	32
2.12	Error between the observed phase speeds and (a) constant $c_0$ (b) analytic function $c_0(y)$ in the Pacific Ocean. Phase speed errors $<0.3\text{ms}^{-1}$ are shown in yellow. . . . .	32
2.13	Error between the observed phase speeds and the analytic function $c_0(x, y)$ . Phase speed errors $<0.3\text{ms}^{-1}$ are shown in yellow. . . . .	33
2.14	Ray paths with variable meridional wavenumber at the boundary and variable $c_0$ for (a) Atlantic Ocean and (b) Pacific Ocean. Red circles indicate latitudes beyond the critical latitude or at which no Rossby wave propagation occurs due to the angle of the coastline. . . . .	34
2.15	Ray paths in spherical polar coordinates for a straight, north-south orientated boundary with a zero initial angular meridional wavenumber . . . . .	38
2.16	Ray paths for (a) the Atlantic Ocean and (b) the Pacific Ocean with a zero meridional wavenumber at boundary. . . . .	40
2.17	Ray paths with variable meridional wavenumber at the boundary and constant gravity-wave phase speed $c_0$ in spherical polar coordinates for (a) the Atlantic Ocean and (b) the Pacific Ocean. Red circles indicate latitudes beyond the critical latitude or at which no Rossby wave propagation occurs due to the angle of the coastline. . . . .	42
2.18	Ray paths with variable meridional wavenumber at the boundary and variable gravity-wave phase speed $c_0$ in spherical polar coordinates for (a) the Atlantic Ocean and (b) the Pacific Ocean. Red circles indicate latitudes beyond the critical latitude or at which no Rossby wave propagation occurs due to the angle of the coastline. . . . .	44
2.19	Caustics in the Atlantic Ocean . . . . .	46
2.20	Caustics in the Pacific Ocean . . . . .	46

3.1	Filtered and unfiltered SSH time series. . . . .	49
3.2	Unfiltered time-longitude plot. . . . .	49
3.3	Filtered time-longitude plot. . . . .	49
3.4	Root mean square variability in the South Atlantic Ocean . . . . .	50
4.1	Challenor et al. (2001) . . . . .	57

# Chapter 1

## Introduction

Rossby wave theory first came about in 1939 (Rossby, 1939) and suggested the existence of westward propagating signals originating primarily from the eastern boundaries of ocean basins. These waves were thought to be the large-scale response of the ocean to wind and buoyancy forcing in the ocean interior and at the eastern boundaries of ocean basins, or due to perturbations along the boundary associated with coastally trapped Kelvin waves originating from the lower latitudes.

Chelton and Schlax (1996) used TOPEX/Poseidon (T/P) satellite altimeter data and confirmed the existence of these waves. They applied a filter to the T/P satellite altimeter data in order to detect sea surface height (SSH) anomalies and therefore single out the oceanic Rossby waves. Having analysed the T/P data, they found that the existing standard linear theory for free, linear Rossby waves was an incomplete description of the observed waves. For example, the westward phase speeds of the observed waves in the mid to high latitudes were significantly greater than those predicted by the linear theory.

The standard linear normal mode theory used for modelling Rossby waves yields an eigenvalue problem with an infinite number of normal mode solutions which are ordered according to their phase speed, the first being the barotropic mode, the second being the first order baroclinic mode and the remaining solutions being higher order baroclinic modes. Barotropic mode waves, having the greatest phase speed, take only days to weeks to cross an ocean basin and behave like ordinary shallow-water gravity waves. Chelton and Schlax (1996), having analysed the T/P data, found that the first order baroclinic mode Rossby waves generally have a surface amplitude of less than 10cm, and a wavelength of at least 500km. Unlike the barotropic mode, the first order baroclinic mode waves take months to decades to cross an ocean basin and have a greater effect on the depth of the thermocline than they do at the surface. The difference in ocean crossing time for a particular

mode of Rossby wave is a result of the latitudinal variation of phase speed. The phase speed's latitudinal dependence is a result of the  $\beta$ -effect, and is thus often referred to as  $\beta$ -refraction, illustrated by Figure (1.1).

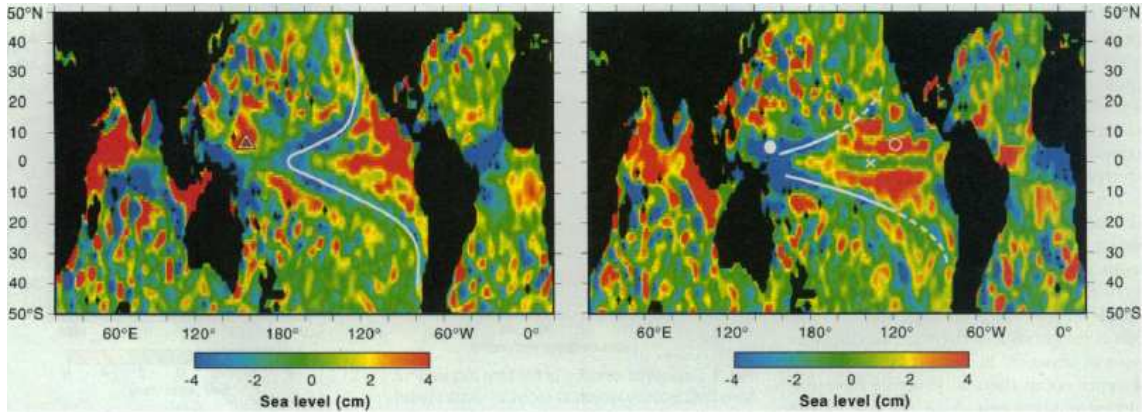


Figure 1.1: White lines identify a westward propagating,  $\beta$ -refracted Rossby wave trough where the two diagrams are separated by a time period of 3 months. The image is taken from Chelton and Schlax (1996) and is based on T/P data.

Barotropic mode Rossby waves take a relatively short amount of time to cross an ocean basin, and thus have little climatic significance. The baroclinic mode waves on the other hand have a very slow propagation speed, taking up to 20 years to cross an entire ocean basin. A baroclinic mode wave with a surface amplitude of 5cm corresponds to a 50m change in depth of the oceanic thermocline, a difference of three orders of magnitude. The slow propagation speed of the baroclinic mode in conjunction with its amplified effect on the thermocline depth means that baroclinic mode waves are an important factor in determining the low-frequency large-scale variability of the ocean interior and thus for decadal-scale climate variability. It is widely believed that the remaining higher order baroclinic modes play a relatively small part in ocean circulation dynamics and we will therefore be concentrating on first-order baroclinic mode Rossby waves in this study.

There are thought to be two primary methods of propagation, boundary-driven waves caused by sea level variability at the eastern boundary of an ocean basin, and wind-driven waves caused by wind stress in the ocean interior. Fu and Qiu (2002) use T/P observational data and suggest that the influence of boundary-driven waves in the North Pacific Ocean has only a limited offshore extent. This extent is dependent on the latitude at which the wave originally propagates, for example an extent of between 3000-4000km at 10°N and between 200-300km at 50°N. Their study also suggests that wind-driven waves seem to overwhelm the boundary-driven waves in the interior ocean and thus that the variability in

the interior is dominated by wind stress. Despite this, they also state from their analysis that the effects of boundary-driven waves are clear when wind-driven variability is removed from the observational data. This can be seen in Figure (1.2) which illustrates correlation coefficients in the North Pacific between observed SSH anomalies and boundary-driven Rossby waves having had wind driven variability removed. The strong correlation that occurs near to the coastline decays rapidly away from the coastline indicating the presence of some significant dissipative or dispersive processes offshore.

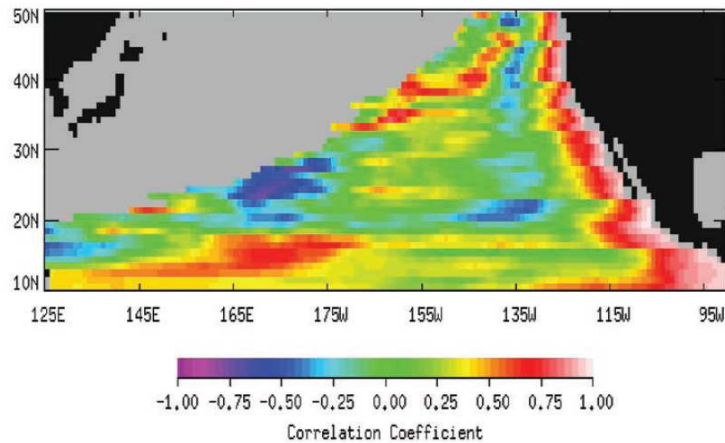


Figure 1.2: Correlation coefficients between SSH variability and boundary-driven Rossby waves having had wind driven anomalies removed from the data (Fu and Qiu, 2002)

Fu and Qiu (2002) suggest that while the short-wavelength Rossby-wave components are susceptible to dissipation soon after propagating from the coast due to their smaller spatial scales, there is still some strong correlation between long-wavelength components from the boundary and SSH variability some distance from the coast. This suggests that the western extent of long-wave propagation is less likely to be limited by dissipation and that dispersion is a more likely cause. The relative importance of boundary-driven and wind-driven waves is still uncertain, however, it is the extent to which boundary-driven Rossby waves can propagate into the western part of an ocean basin that we are interested in. In this study we will consider dispersion as the possible underlying mechanism of this limited offshore extent.

One fundamental property of waves is that they can transmit energy over great distances through the disturbances that they create. Consider the presence of many different wave disturbances in the ocean. The interference of these wave disturbances with one another creates a beat pattern known as a wave group or packet. The wave group is enclosed by a wave envelope which has an overall amplitude of  $A(x)$  and contains individual disturbances of wavelength  $\lambda$ . The local value of the wave envelope amplitude is determined by

individual crests and troughs of the disturbances contained within it.

While an individual wave disturbance travels at its own phase speed, a wave envelope, illustrated by Figure (1.3) travels at the group velocity. The significance of this is that wave energy is conserved and propagates with the wave group at the group velocity as opposed to the phase speed (Pedlosky, 1986). The amplitude of the wave envelope therefore determines where there is significant wave energy where for example, a small wave amplitude indicates limited wave activity. If the group velocity of the wave envelope is not equal to the phase speed of the individual wave crests and troughs, then the waves are dispersive. A result of this is that the motion of a Rossby wave packet can be determined using the Rossby wave dispersion relationship.

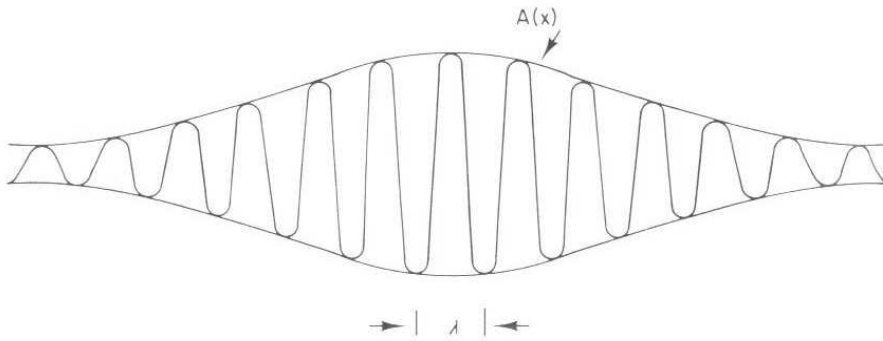


Figure 1.3: A wave envelope.

Schopf et al. (1981) investigated the dispersion of annual and semi-annual frequency oceanic Rossby waves by examining the group velocity vector. The study used the Rossby wave dispersion relationship and ray theory (defined later) to derive a system of differential equations that could describe the group velocity of a Rossby wave packet. It was found that, in general, group velocity vectors originating at some distance from the equator on a straight, north-south orientated boundary, would turn and propagate equatorwards. This is illustrated by Figure (1.4). The turning of the rays occurs as a result of the latitudinal variability of the Rossby Radius of deformation and suggests that Rossby waves originating from high latitudes are able to disperse into the equatorial zone. This suggests that energy from Rossby waves originating in the high latitudes is transported equatorwards as opposed to the western part of the ocean basin and thus that there is a limited extent to which boundary driven waves can propagate westwards at some latitudes. This extent is marked by a theoretical line called a caustic line.

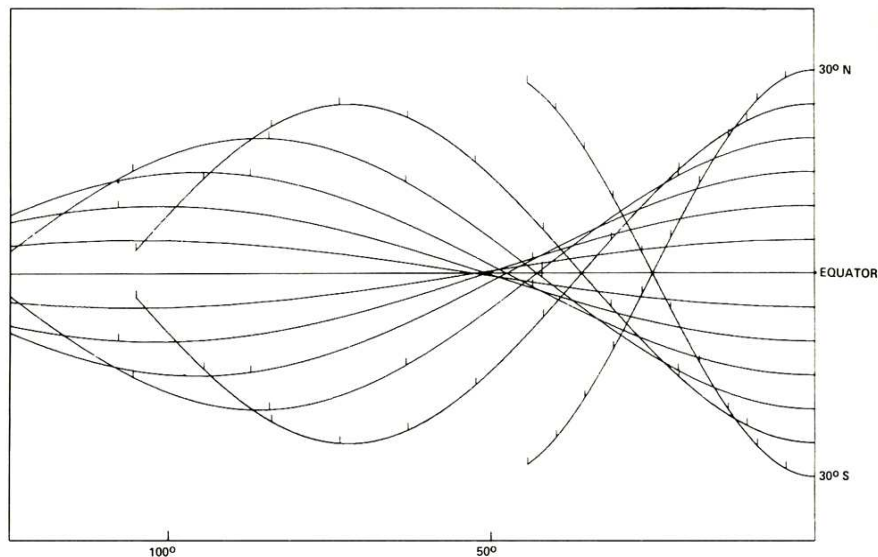


Figure 1.4: A simple example of a ray propagation pattern from a straight, north-south orientated boundary for semi-annual frequency Rossby waves (Schopf et al. 1981).

Grimshaw and Allen (1983) discuss the existence of a critical latitude  $\phi_c$  polewards of which waves remain coastally trapped as poleward propagating internal Kelvin waves and equatorwards of which trapped waves can still exist, but waves can also propagate freely as offshore propagating baroclinic Rossby waves. The critical latitude is strongly dependent on the frequency of the waves such that there is also a critical frequency  $\omega_c$  for which coastally trapped Kelvin waves may or may not propagate as a Rossby wave. This study also used the method of characteristics or rays and suggests the existence of a caustic line which originates at the intersection between the coastline and critical latitude, and polewards of which Rossby waves propagating from the eastern boundary decay exponentially. Rossby wave dispersion is the principal cause for the existence of this caustic line.

The studies by Schopf et al. (1981) and Grimshaw and Allen (1983) considered straight eastern boundaries and used the  $\beta$  approximation to derive solutions in cartesian coordinates. Each of them suggest that wave dispersion is likely to result in a limited western extent of Rossby wave propagation, an extent that has been observed in studies such as Fu and Qiu (2002). The aim of this project is to revisit the methods used in the aforementioned studies and examine ray propagation, particularly from the Atlantic and Pacific coastlines. A model will be derived to calculate the paths of the Rossby wave rays initially on the equatorial  $\beta$ -plane, and then in spherical polar coordinates in order to account for the curvature of the Earth. While previous studies have assumed that the baroclinic

gravity-wave phase speed is constant, we will introduce an analytical function representative of a more realistic phase speed distribution. This will yield an original result and allow us to examine the effect of a variable phase speed on ray propagation. From the ray solutions, we can gain a visual picture of the potential location of the caustics described in the literature. We will then attempt to locate real caustics in modelled SSH data and compare any results with the theoretical predictions produced from the ray solutions.

## 1.1 Theory

### 1.1.1 A Note On WKB Theory

The Wentzel-Kramers-Brillouin (WKB) approximation involves recasting a wavefunction as an exponential function, expanding the resulting function and multiplying higher derivatives by a small parameter  $\epsilon$ . Usually either the wave amplitude or phase speed is taken to be slowly varying. For our purposes, we will take the wave amplitude to be slowly varying. The WKB approximation is valid provided that the scale of the spatial variations is large compared with the wavelength of the waves being examined (Schopf et al. 1981).

### 1.1.2 Dispersion Relationship

In order to derive our model equations, we begin with the Quasi-Geostrophic potential vorticity conservation (QGPVC) equation on a  $\beta$ -plane.

$$\frac{\partial}{\partial t} \left( \Delta \Psi - \frac{1}{R^2} \Psi \right) + \beta \frac{\partial \Psi}{\partial x} = 0 \quad (1.1)$$

where

$$\Delta \Psi = \frac{\partial^2 \Psi}{\partial x^2} + \frac{\partial^2 \Psi}{\partial y^2} \quad (1.2)$$

Here  $R = c_0/f$  is the Rossby radius of deformation where  $c_0$  is the equivalent gravity wave speed and  $f = \beta y$  is the coriolis parameter under the  $\beta$ -plane approximation. The equation admits plane wave solutions of the form:

$$\Psi = A \exp i [k_x x + k_y y - \omega t] \quad (1.3)$$

where  $k_x$  and  $k_y$  are the zonal and meridional wavenumbers respectively and  $\omega$  is the wave's angular frequency. We derive the Rossby wave dispersion relationship by substituting the plane wave solution  $\Psi$  into the QGPVC equation.

From Equation (1.1) we can therefore write:

$$\frac{\partial}{\partial t} \left[ - (k_x^2 + k_y^2) \Psi - \frac{1}{R^2} \Psi \right] + \beta i k_x \Psi = 0 \quad (1.4)$$

$$\Rightarrow i\omega (k_x^2 + k_y^2) + \frac{i\omega}{R^2} + \beta i k_x = 0 \quad (1.5)$$

$$\Rightarrow [1 + R^2 (k_x^2 + k_y^2)] \omega + \beta R^2 k_x = 0 \quad (1.6)$$

Thus we arrive at the Rossby wave dispersion relationship for a plane wave solution:

$$\omega = \frac{-\beta R^2 k_x}{1 + R^2 (k_x^2 + k_y^2)} \quad (1.7)$$

The plane wave solution involves the rather unrealistic assumption that the wave field is strictly periodic with a constant amplitude. It is mostly used as a local approximation to the true wave dynamics. Examining the transmission of a wave disturbance requires consideration of wave fields where the wave amplitude is no longer constant but also a function of time and space.

Let us now consider wave solutions of a slightly different form:

$$\Psi = A(x, y, t) e^{iS(x, y, t)} \quad (1.8)$$

where the wave amplitude  $A$  is a slowly varying function of  $x$ ,  $y$  and  $t$  (roughly constant over one wavelength) in comparison to the phase function  $S$  and where  $S = k_x x + k_y y - \omega t$ . According to ray theory, the zonal and meridional wavenumbers  $k_x$  and  $k_y$ , and angular frequency  $\omega$ , are defined as derivatives of the phase function:

$$\omega = -\frac{\partial S}{\partial t} \quad (1.9)$$

$$k_x = \frac{\partial S}{\partial x} \quad (1.10)$$

$$k_y = \frac{\partial S}{\partial y} \quad (1.11)$$

We now look to show that this satisfies the same dispersion relationship by substituting this wave solution into the QGPVC equation and using the equations defined above.

It can be shown that:

$$\frac{\partial \Psi}{\partial x} = \frac{\partial A}{\partial x} e^{iS} + Ai \frac{\partial S}{\partial x} e^{iS} \quad (1.12)$$

$$\frac{\partial \Psi}{\partial y} = \frac{\partial A}{\partial y} e^{iS} + Ai \frac{\partial S}{\partial y} e^{iS} \quad (1.13)$$

$$\Delta \Psi = \left( \frac{\partial^2 A}{\partial x^2} + \frac{\partial^2 A}{\partial y^2} \right) e^{iS} + 2i \left( \frac{\partial A}{\partial x} \frac{\partial S}{\partial x} + \frac{\partial A}{\partial y} \frac{\partial S}{\partial y} \right) e^{iS} - A \left( \frac{\partial^2 S}{\partial x^2} + \frac{\partial^2 S}{\partial y^2} \right) e^{iS} \quad (1.14)$$

Now we consider that  $A=A[X, Y, T]$  where  $X=\epsilon x$ ,  $Y=\epsilon y$ ,  $T=\epsilon t$  and  $\epsilon$  is a small term since we have taken  $A$  to be a slowly varying function in time and space. We can therefore rewrite some of the terms above, for example:

$$\frac{\partial A}{\partial x} = \frac{\partial A}{\partial X} \frac{\partial X}{\partial x} = \epsilon \frac{\partial A}{\partial X} \quad (1.15)$$

and ignore them due to their relatively small magnitude so that only the lowest order terms remain. We are left with:

$$\Delta \Psi = - \left( \frac{\partial^2 S}{\partial x^2} + \frac{\partial^2 S}{\partial y^2} \right) \Psi \quad (1.16)$$

From equation (1.1) we can now write:

$$\frac{\partial}{\partial t} \left[ - \left( \frac{\partial^2 S}{\partial x^2} + \frac{\partial^2 S}{\partial y^2} \right) \Psi - \frac{1}{R^2} \Psi \right] + \beta i \frac{\partial S}{\partial x} \Psi \quad (1.17)$$

and from equations (1.10) and (1.11) it is clear that this is equivalent to:

$$\frac{\partial}{\partial t} \left[ - (k_x^2 + k_y^2) \Psi - \frac{1}{R^2} \Psi \right] + \beta i k_x \Psi = 0 \quad (1.18)$$

$$\omega [-R^2 (k_x^2 + k_y^2) - 1] + \beta k_x = 0 \quad (1.19)$$

We therefore arrive at the same relationship as given by equation (1.7):

$$\omega = \frac{-\beta R^2 k_x}{1 + R^2 (k_x^2 + k_y^2)} \quad (1.20)$$

We have thus shown that the basic notions developed for plane waves are directly applicable to a slowly varying wave packet and therefore that the derived dispersion relationship in the first approximation (using only the lowest order terms) is equal to that used for a pure plane wave solution.

### 1.1.3 Ray Equations

Although the phase speed of a Rossby wave is almost always directed purely westward, the group velocity has no such restriction. As the energy associated with Rossby waves propagates with the group velocity  $c_g$  of a wave packet, it is therefore important to calculate the group velocity when examining energy propagation. Ray tracing is when we define a set of points in the direction of the group velocity such that energy propagates through them with a velocity equal to the group velocity. A ray is obtained from the numerical integration of the group velocity given some initial position  $(x_0, y_0)$ . From Leblond (1978) we can define the following standard relationship, also known as the Conservation of Crests equation:

$$\frac{\partial \mathbf{k}}{\partial t} + \nabla \omega = 0 \quad (1.21)$$

where  $\mathbf{k}$  is the vector containing the zonal and meridional wavenumbers  $(k_x, k_y)^T$ . We can separate this equation into its individual components:

$$\frac{dk_x}{dt} = -\frac{\partial \omega}{\partial x} \quad (1.22)$$

$$\frac{dk_y}{dt} = -\frac{\partial \omega}{\partial y} \quad (1.23)$$

The only way that the dispersion relationship can depend on  $x$  is if the phase speed  $c_0$  is also dependent on  $x$  and thus if  $c_0 = c_0(x)$  or  $c_0 = c_0(x, y)$ . In this project however, we will generally consider either a constant phase speed or the phase speed function  $c_0 = c_0(y)$  which depends on  $y$  only. In this case, we can assume that the zonal wavenumber does not change from its initial value, but rather is conserved along each ray:

$$\frac{dk_x}{dt} = 0 \quad (1.24)$$

Finally, the zonal and meridional group velocities of the wave are:

$$\frac{dx}{dt} = \frac{\partial \omega}{\partial k_x} = c_{gx} \quad (1.25)$$

$$\frac{dy}{dt} = \frac{\partial \omega}{\partial k_y} = c_{gy} \quad (1.26)$$

Equations (1.22), (1.23), (1.25) and (1.26) will provide the basis of our model. We will begin however by considering the analytical solution derived by Schopf et al. (1981) and then Grimshaw and Allen (1983).

### 1.1.4 Analytical Solution

For the most simple case, an analytical solution can be derived to describe the ray paths. The most simple case relies on a few basic assumptions, that waves are propagating from a straight, north-south orientated eastern boundary, that the gravity-wave phase speed  $c_0$  is constant, and that the phase function  $S$  is constant along the eastern boundary. We start by rearranging the dispersion relationship into the following form:

$$\left(k_x + \frac{\beta}{2\omega}\right)^2 + k_y^2 = \frac{\beta^2}{4\omega^2} - \frac{f^2}{c_0^2} \quad (1.27)$$

Under the assumption that the wave amplitude is slowly varying compared to variations in the phase, it is possible to use WKB ideas. We therefore refer back to and redefine equations (1.10) and (1.11), which under WKB theory mean that the locally defined wavenumbers must satisfy the dispersion relationship  $\omega$ :

$$\begin{aligned} k_x &= \frac{\partial S}{\partial x} \\ k_y &= \frac{\partial S}{\partial y} \end{aligned} \quad (1.28)$$

From equation (1.28), an added constraint is that the wavenumbers must also satisfy the following compatibility condition:

$$\frac{\partial k_x}{\partial y} = \frac{\partial k_y}{\partial x} \quad (1.29)$$

If we consider Rossby waves of a constant frequency, we need only solve equations for the wavenumbers  $k_x$  and  $k_y$  and not  $\omega$ . Differentiating equation (1.27) with respect to  $x$  yields:

$$2k_x \frac{\partial k_x}{\partial x} + \frac{\beta}{\omega} \frac{\partial k_x}{\partial x} + 2k_y \frac{\partial k_y}{\partial x} = 0 \quad (1.30)$$

This is equivalent to:

$$\left(k_x + \frac{\beta}{2\omega}\right) \frac{\partial k_x}{\partial x} + k_y \frac{\partial k_y}{\partial x} = 0 \quad (1.31)$$

Using the compatibility condition specified by equation (1.29), this can be written as follows:

$$\left(k_x + \frac{\beta}{2\omega}\right) \frac{\partial k_x}{\partial x} + k_y \frac{\partial k_x}{\partial y} = 0 \quad (1.32)$$

This equation takes on the form of a quasi-linear first order partial differential equation:

$$a(x, y, k_x) \frac{\partial k_x}{\partial x} + b(x, y, k_x) \frac{\partial k_x}{\partial y} = c(x, y, k_x) \quad (1.33)$$

where

$$\begin{aligned} a &= k_x + \frac{\beta}{2\omega} \\ b &= k_y \\ c &= 0 \end{aligned} \quad (1.34)$$

We define the ray trajectory for which we want to solve as the curve  $\mathbf{r}(x(t), y(t), k_x(t))$  which must satisfy:

$$\frac{d\mathbf{r}}{dt} = (a, b, c) \quad (1.35)$$

It is clear that equation (1.35) represents a system of differential equations that describes the path of group velocity and variations in the zonal and meridional wavenumbers of the Rossby waves:

$$\frac{dx}{dt} = k_x + \frac{\beta}{2\omega} \quad (1.36)$$

$$\frac{dy}{dt} = k_y \quad (1.37)$$

$$\frac{dk_x}{dt} = 0 \quad (1.38)$$

$$\frac{dk_y}{dt} = -\frac{\beta f}{c_0^2} \quad (1.39)$$

The equation for the ray trajectory is therefore given by:

$$\frac{dy}{dx} = \frac{k_y}{k_x + \beta/(2\omega)} \quad (1.40)$$

As we have assumed a constant frequency,  $\omega = \omega_0$  and clearly from equation (1.38),  $k_x = k_{x0}$  remains constant along each ray. The remaining solutions to the ray equations, as derived by Grimshaw and Allen (1983), are given as follows:

$$x = x_0 + \left( k_x + \frac{\beta}{2\omega} \right) t \quad (1.41)$$

$$y = y_0 \cos \left( \frac{\beta t}{c_0} \right) \quad (1.42)$$

$$k_y = -\frac{\beta y_0}{c_0} \sin\left(\frac{\beta t}{c_0}\right) \quad (1.43)$$

where  $x_0$  and  $y_0$  are the coordinates of the starting point of the ray trajectory. Using the equations for  $x$  and  $y$ , a constant gravity-wave phase speed of  $c_0 = 3\text{ms}^{-1}$  and specifying  $\omega$  such that it corresponds to semi-annual frequency Rossby waves, we can immediately reproduce the solution derived by Schopf et al. (1981) propagating from a straight north-south orientated boundary. This is illustrated by Figure (1.5).

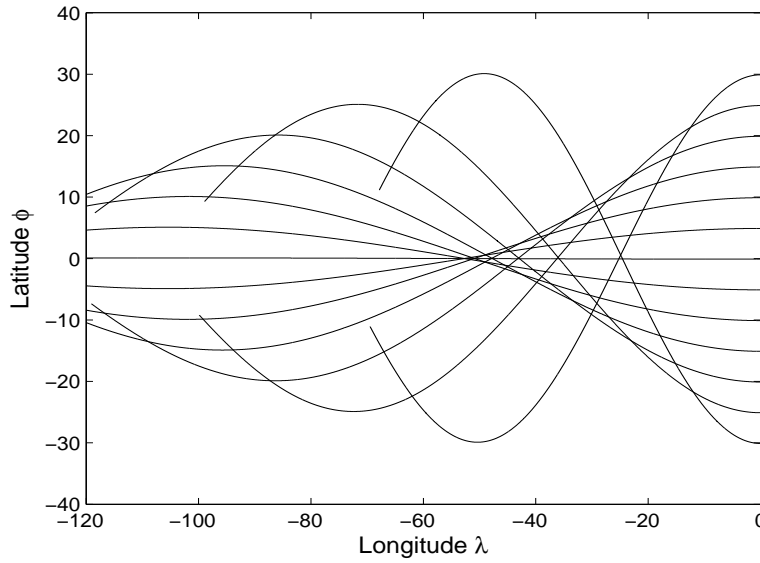


Figure 1.5: Analytic solution from equations (1.41) and (1.42) for semi-annual frequency Rossby waves.

Suppose  $\xi$  is a measure of distance along the eastern boundary from which a ray trajectory begins. A caustic appears when two neighboring trajectories from  $\xi$  and  $\xi + \delta\xi$  reach the same location at the same time, i.e. when:

$$\begin{aligned} x(t, \xi) &= x(t + \delta t, \xi + \delta\xi) \\ y(t, \xi) &= y(t + \delta t, \xi + \delta\xi) \end{aligned} \quad (1.44)$$

This is satisfied only when:

$$\frac{\partial x}{\partial \xi} = \frac{\partial y}{\partial \xi} = 0 \quad (1.45)$$

At the point where two rays meet, the ray amplitude and thus energy of the wave under

consideration becomes infinite. This is an unphysical result and indicates a failure of the ray theory. For the purpose of Rossby wave dispersion the caustic acts as an envelope. Within the envelope, WKB theory remains valid and thus there are real ray solutions. On the caustic WKB theory breaks down, and westward of it Rossby waves decay exponentially. As we expect ray theory to be valid within the envelope, we also expect Rossby wave propagation to occur within this region. We do not expect any boundary driven Rossby rays to propagate beyond the caustic.

While it has been shown that there is an analytical solution for the most simple case, i.e. a straight boundary, constant gravity wave phase speed, all under the  $\beta$ -plane approximation, we intend to extend the ideas to account for variable phase speed, realistic coastlines, and eventually to spherical polar coordinates. For this reason we will concentrate on using numerical solution to solve the differential equations for the remaining part of the project.

## Chapter 2

# Model Derivation and Results

In this section, we will derive the model, initially in cartesian coordinates and then in spherical polar coordinates. The model involves solving a system of ordinary differential equations which will be done using the Matlab ODE solver. More specifically we shall use the ODE45 solver, which uses the 4<sup>th</sup>-Order Runge-Kutta method. We will first assume that the eastern boundary is straight and north-south orientated, and that the equivalent gravity wave speed  $c_0$  is constant. We will then examine the effect of removing these assumptions on the ray solutions, and consider the impacts of converting to spherical polar coordinates. Finally, we will try to locate the potential paths of the caustics in both hemispheres for the Atlantic and Pacific Oceans.

### 2.1 Cartesian Coordinates

#### 2.1.1 Ray Equations

The ray equations for our model in cartesian coordinates are:

$$\frac{dx}{dt} = c_{gx} = \frac{\partial \omega}{\partial k_x} = -\frac{\beta R^2 [1 + R^2 (k_y^2 - k_x^2)]}{[1 + R^2 (k_x^2 + k_y^2)]^2} \quad (2.1)$$

$$\frac{dy}{dt} = c_{gy} = \frac{\partial \omega}{\partial k_y} = \frac{2\beta R^4 k_x k_y}{[1 + R^2 (k_x^2 + k_y^2)]^2} \quad (2.2)$$

$$\frac{dk_x}{dt} = -\frac{\partial \omega}{\partial x} = 0 \quad (2.3)$$

$$\frac{dk_y}{dt} = -\frac{\partial \omega}{\partial y} = -\frac{2\beta^2 R^2 k_x}{f [1 + R^2 (k_x^2 + k_y^2)]^2} \quad (2.4)$$

While we are working in cartesian coordinates, we will take  $x$  to be longitude and  $y$  to be

latitude, where for example  $y = 1000\text{km}$  or  $y = -1000\text{km}$  represents a position 1000km north or south of the equator respectively. Under the  $\beta$ -approximation, we make the assumption that the  $\beta$ -parameter is constant, and thus that the Coriolis parameter  $f = \beta y$  varies linearly with latitude. We approximate  $\beta$  with:

$$\beta \approx \frac{2\Omega}{a} \approx 2.288 \times 10^{-11} \text{m}^{-1} \text{s}^{-1} \quad (2.5)$$

where  $a = 6371\text{km}$  is the mean Earth radius and  $\Omega = 2\pi\text{day}^{-1}$  is Earth's rate of rotation.

From equation (2.1), it is clear that the group velocity in the  $x$ -direction,  $c_{gx}$  can be either positive or negative. The sign of  $c_{gx}$  is dependent on the the following condition. If we have that:

$$1 + R^2 (k_y^2 - k_x^2) < 0 \quad (2.6)$$

then the group velocity in the  $x$ -direction is clearly positive, since it is known that  $\beta > 0$ . From Pedlosky (2003), waves of this specification are short waves. If on the other hand, we have that:

$$1 + R^2 (k_y^2 - k_x^2) > 0 \quad (2.7)$$

then the group velocity is negative. Thus long waves, which we are primarily interested in, have their energy propagate westwards.

### 2.1.2 Autonomous Equations

When solving these equations with Matlab's built in ODE solver, we come across a problem. Towards the equator, it is the case that  $y \rightarrow 0$  and the Rossby radius of deformation  $R \rightarrow \infty$  as  $y \rightarrow 0$  since it is a function of the recipricol of  $y$ . This poses a problem when we integrate these equations with time, as the rays close to the equator shoot off to infinity, and this makes it difficult to produce a suitable plot of rays across a diverse range of latitudes. As we will be considering the long wave solution of the ray equations, we can assume from equations (2.1) and (2.7) that the group velocity in the  $x$ -direction will be negative everywhere, i.e.  $c_{gx} < 0$ . A result of this is that we can avoid any problems when solving near to the equator by integrating the equations with respect to  $x$  as opposed to  $t$ . By removing the independent variable  $t$ , we reduce our system of differential equations to an autonomous system and we can integrate for each ray trajectory between the eastern boundary and some specified western extent.

The autonomous system is derived as follows. We know from equation (2.1):

$$\frac{dx}{dt} = c_{gx} \quad (2.8)$$

We can therefore write that:

$$dt = \frac{dx}{c_{gx}} \quad (2.9)$$

Using this, we can rewrite equations (2.2) and (2.4) as follows:

$$\frac{dy}{dx} = \frac{c_{gy}}{c_{gx}} \quad (2.10)$$

$$\frac{dk_y}{dx} = \frac{1}{c_{gx}} \frac{dk_y}{dt} \quad (2.11)$$

Thus our autonomous system of differential equations is given by:

$$\frac{dy}{dx} = \frac{-2R^2 k_x k_y}{[1 + R^2 (k_y^2 - k_x^2)]} \quad (2.12)$$

$$\frac{dk_x}{dx} = 0 \quad (2.13)$$

$$\frac{dk_y}{dx} = \frac{2\beta k_x}{f [1 + R^2 (k_y^2 - k_x^2)]} \quad (2.14)$$

One disadvantage of integrating spatially as opposed to temporally is that we cannot see the time evolution of the rays. However the time evolution of the rays is not significant if we are simply trying to determine the caustics separating the region of wave propagation and the region of no wave propagation. In general, the autonomous system has one less equation and is therefore not only a means by which we can avoid any problems that crop up through integrating with time, but is also more simple to solve.

### 2.1.3 Fixed $k_x$ Solution

We can now integrate equations (2.12) and (2.14) to find a simple solution of the ray paths. We do not need to solve a differential equation for  $k_x$  since equation (2.13) simply implies that  $k_x$  retains its initial value along each ray solution. We will first assume that while the frequency  $\omega$  varies along the coastline, the zonal wavenumber  $k_x$  has a fixed value of  $k_x = 9 \times 10^{-6} \text{m}^{-1}$  and is constant in all equations.

We will solve for ray trajectories beginning from a straight north-south eastern boundary,

in which case we take as a boundary condition that the phase,  $S$  is constant along the boundary. In this case it can be shown that:

$$\frac{\partial S}{\partial y} = k_y = 0 \quad (2.15)$$

The meridional wavenumber  $k_y$  will therefore have a zero initial value for each ray trajectory. This assumption is valid only while the coastline is straight and has a north-south orientation, but not in the more general case of a variable coastline. The initial value of  $x$  will also be zero and we will calculate ray solutions for a range of initial values of  $y$ . Finally, having calculated the global average baroclinic gravity-wave phase speed for oceanic Rossby waves from the Chelton et al. (1998) data set, we will initially take  $c_0$  to have a constant value of  $2.6\text{ms}^{-1}$ .

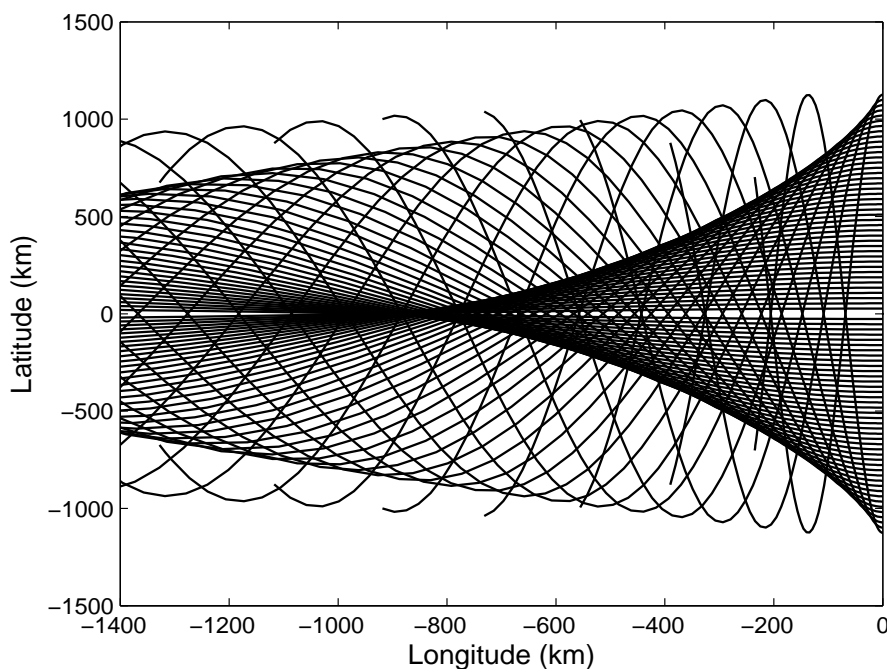


Figure 2.1: Ray paths from a straight boundary with a fixed  $k_x$

Having integrated the equations for group velocity, we get some preliminary results of the ray paths with a straight north-south boundary. Figure (2.1) is a graphical representation of the ray equation solutions. We integrate over a range of latitudes in order to get a full picture of the energy propagation pattern. It is clear that rays propagating from the poleward latitudes are primarily directed equatorwards, whereas rays near to the equator are directed almost purely westward. The dark boundary enclosing the majority of the ray

solutions is known as the caustic line which we will discuss in more detail later. Important to note is the symmetry of the solution about the equator.

#### 2.1.4 Fixed $\omega$ Solution

We will now no longer assume that  $k_x$  is fixed at the boundary but instead fix  $\omega$ . By doing this we can specify the particular Rossby wave frequency for which we are solving the differential equations. Fixing  $\omega$  means that we need to solve for the initial value of  $k_x$  at the eastern boundary. Keeping in mind that from equation (2.15), we are using an initial value of  $k_y = 0$  we can write the dispersion relationship along the boundary as:

$$\omega = \frac{-\beta R^2 k_x}{1 + R^2 k_x^2} \quad (2.16)$$

$$\omega (1 + R^2 k_x^2) + \beta R^2 k_x = 0 \quad (2.17)$$

$$R^2 k_x^2 + \frac{\beta R^2}{\omega} k_x + 1 = 0 \quad (2.18)$$

This is equivalent to:

$$R^2 k_x^2 + \frac{R c_0}{\omega y} k_x + 1 = 0 \quad (2.19)$$

since  $R = c_0/\beta y$ . This is simply a quadratic equation for  $k_x$  which can easily be solved to give the value of  $k_x$  along each ray. The quadratic equation yields two solutions, one corresponding to long waves, and the other to short waves:

$$k_x^{long} = \frac{-\beta R + \sqrt{\beta^2 R^2 - 4\omega^2}}{2R\omega} \quad (2.20)$$

$$k_x^{short} = \frac{-\beta R - \sqrt{\beta^2 R^2 - 4\omega^2}}{2R\omega} \quad (2.21)$$

In this study, we will concentrate explicitly on the long wave solution.

We can now compare the analytical solution as in Figure (1.5), with the numerical solution derived from the autonomous system of differential equations for semi-annual frequency Rossby waves. The comparison is illustrated by Figure (2.2) and indicates that there is very little error associated with the 4<sup>th</sup>-order Runge-Kutta method. The shape of the ray envelope is the same, and noticeably sized errors only begin to appear in the far west where they are not as important. We will therefore continue to use the Matlab ODE45 solver.

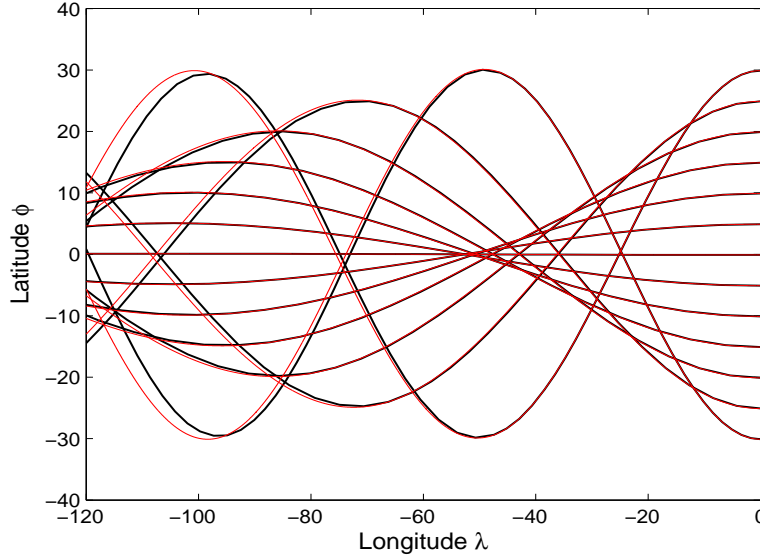


Figure 2.2: Comparison of analytical (red) and numerical (black) solution for semi-annual frequency oceanic Rossby waves.

### 2.1.5 Critical Latitude

It is clear that to avoid a complex solution of equation (2.19), the following condition must be satisfied:

$$\beta^2 R^2 - 4\omega^2 > 0 \quad (2.22)$$

From this we can calculate the maximum frequency for which Rossby wave propagation can occur from the eastern boundary:

$$\omega_{max} = \frac{\beta c_0}{2f} = \frac{c_0}{2y} \quad (2.23)$$

We will focus on annual frequency Rossby waves so that  $\omega = 2 \times 10^{-7} s^{-1}$  and continue to assume that the gravity-wave phase speed simply takes on the global average such that  $c_0 = 2.6 \text{ms}^{-1}$  and is constant in time and space. As we are considering Rossby waves of an annual frequency, we are less interested in the maximum frequency  $\omega_{max}$  and more interested in the critical latitude ( $y_c$  in cartesian coordinates). It can be shown that for an incident low-frequency wave with a fixed frequency  $\omega$ , there exists some critical latitude polewards of which waves remain coastally trapped as Kelvin waves. Equatorwards of the critical latitude, waves can propagate offshore as Rossby waves. It is clear that from rewriting equation (2.23), the critical latitude is given by:

$$y_c = \frac{c_0}{2\omega} \quad (2.24)$$

since we need a real value of the zonal wavenumber  $k_x$  for Rossby wave propagation to occur. At this stage, the critical latitude simply depends on the gravity wave phase speed  $c_0$  and angular frequency  $\omega$ . For Rossby waves of an angular frequency, assuming a uniform phase speed of  $c_0 = 2.6\text{ms}^{-1}$ , it can be shown that the critical latitude  $y_c$  for a fixed  $\omega$  solution and a straight boundary is approximately  $y_c = 6525\text{km}$ . This is illustrated by Figure (2.3) below. Polewards of the critical latitude, values of  $k_x$  are complex, and thus the rays north of the red dashed line in Figure (2.3) are derived from the real part of the zonal wavenumber. No wave propagation occurs at these latitudes. Also note once more, the symmetry of the ray pattern about the equator.

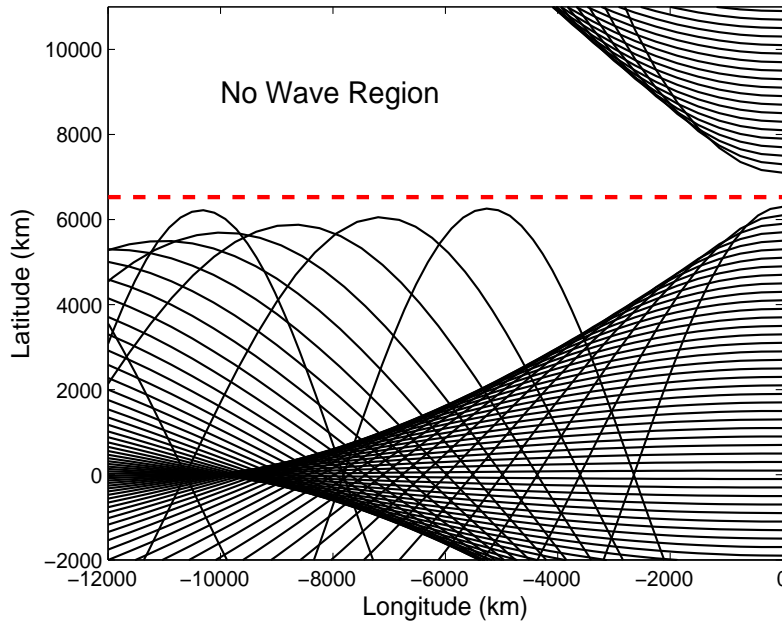


Figure 2.3: Fixed  $\omega$  solution focused on the northern hemisphere. The red dashed line represents the critical latitude  $y_c$  north of which no waves propagate from the eastern boundary.

Schopf et al. (1981) suggests that for a north-south orientated coastline, there is an almost exact focus of wave energy near to the equator at a distance of:

$$x = -\pi c_0 / 4\omega \quad (2.25)$$

from the eastern boundary. As we are considering waves of an annual frequency with a phase speed of  $2.6\text{ms}^{-1}$ , it can be shown that this focus of energy should be approximately

10250km from the eastern boundary, a result consistent with the graphical representation given in Figure (2.3). The location of this energy focus is expected to be an area of very intense Rossby wave activity.

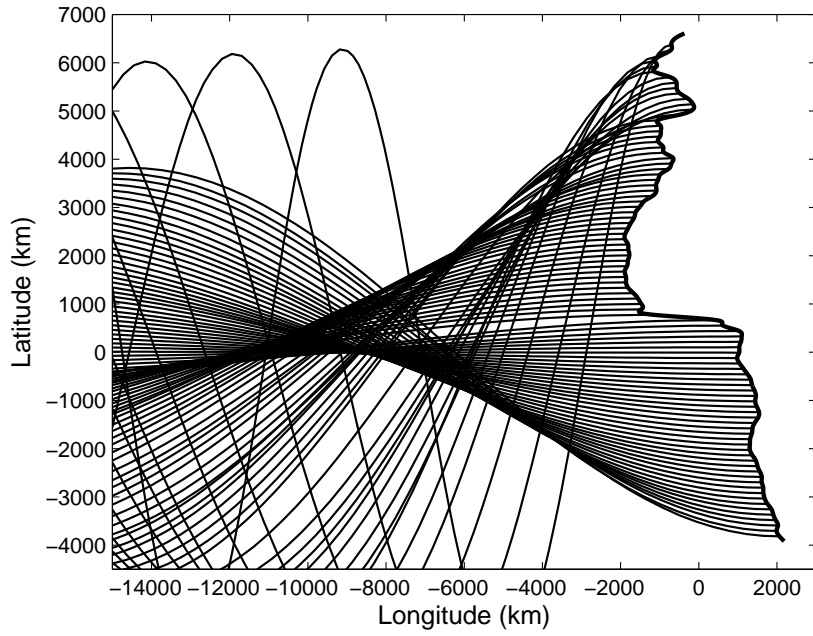
### 2.1.6 Realistic Coastlines

Thus far we have only considered wave propagation from a straight, north-south boundary. Now we extend our model to account for realistic coastline geometry by introducing two vectors with  $x$  and  $y$  coordinates such that they follow the eastern coastlines of the Atlantic and Pacific Oceans. Coastline coordinates were taken every  $1^\circ$  of latitude and to keep the coastlines smooth, points between were calculated using the inbuilt Matlab interpolation function. It is important to consider that we are using relatively smooth, simplified coastline geometry such that complicating features such as islands are not taken into account. We define the equation representing the coastline as:

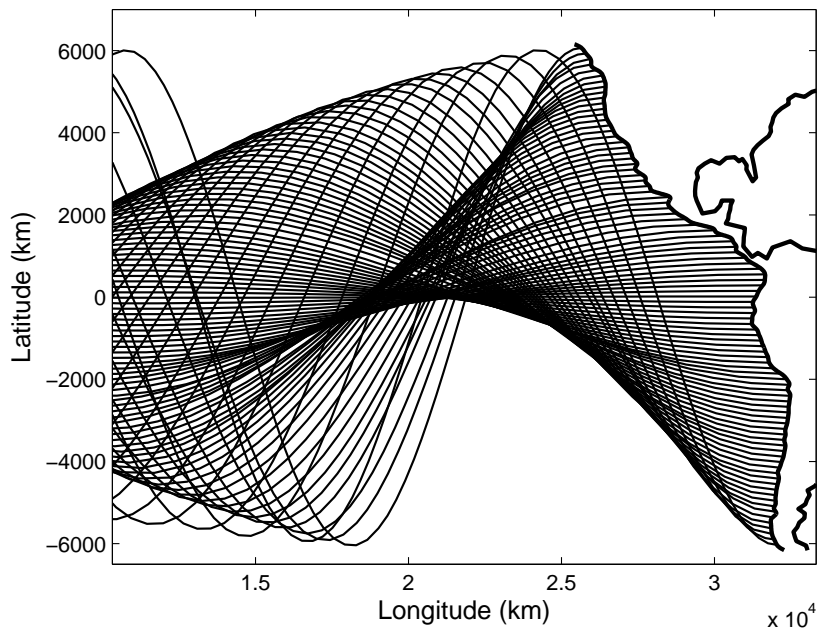
$$x = X_e(y) \tag{2.26}$$

We then use the coastline coordinates to specify the initial values  $x_0$  and  $y_0$  in the model equations, so that we are integrating from the coastline. It is important to note that in the Atlantic Ocean, we set the Greenwich Meridian to be zero longitude. We use negative and positive values of longitude to indicate locations that are East or West of the meridian in the Atlantic. In the Pacific Ocean however, we take the longitude to be the distance eastwards of the Greenwich Meridian, such that it is always positive. For the time being we shall also omit the western coastline from figures so that we can examine the properties of the entire ray envelope.

The resulting solutions for the Atlantic and Pacific oceans with constant phase speed and  $k_y = 0$  along the boundary are shown in Figure (2.4). The effect of the addition of coastline geometry is significant. There are now obvious asymmetries present in the solution about the equator relative to the straight boundary solution and these asymmetries are most obvious where there are large longitudinal distances between values of  $x_0$  for adjacent values of  $y_0$ . For example, the effect of the eastern coastline of Africa just north of the equator is clearly visible in the ray solutions almost directly to the west. Using constant  $c_0 = 2.6\text{ms}^{-1}$  and  $k_y = 0$  along the boundary means that the critical latitude remains at about 6525km in either hemisphere, which lies beyond the coastline geometry for the Pacific coastline and most of the Atlantic coastline with the exception of the northern most part of the coast in the Atlantic. As we shall see however, using constant values for  $c_0$  and  $k_y$  are assumptions that can only be retained for the most basic model solution.



(a) Atlantic Ray Paths



(b) Pacific Ray Paths

Figure 2.4: Ray solutions for (a) Atlantic and (b) Pacific coastline geometry under the assumption of a zero meridional wavenumber along the boundary and constant  $c_0$ .

### 2.1.7 Variable Meridional Wavenumber

Now that we are considering variable coastline geometry, we can no longer use the same boundary condition specified by equation (2.15) which specifies a zero meridional wavenumber along the boundary. We need to impose a boundary condition for the phase along the eastern boundary  $X_e(y)$ . Consider a vector  $\mathbf{l}_s$  which is a projection of the wavenumber vector along the coastline. The initial wavenumber  $\mathbf{k} = (k_x, k_y)$  has to satisfy not only the dispersion relationship but also the following condition given by Schopf et al. (1981):

$$\mathbf{l}_s = \mathbf{k} \cdot \mathbf{e}_s$$

where  $\mathbf{e}_s$  is the unit vector along the coast. This imposes the following condition on the initial zonal and meridional wavenumbers:

$$k_y = -k_x \frac{dX_e}{dy} \quad (2.27)$$

where  $dX_e/dy = -\tan\alpha$  and  $\alpha$  is the angle between the coastline and the meridian. An coastline angle of  $\alpha = 0$  therefore corresponds to the case of a north-south eastern boundary,  $\alpha > 0$  corresponds to a north-east sloping boundary and  $\alpha < 0$  corresponds to a north-west sloping boundary. In this case we must also form a new equation for the zonal wavenumber before the meridional wavenumber can subsequently be calculated. We first rewrite the dispersion relationship:

$$\omega = -\frac{\beta R^2 k_x}{1 + R^2 k_x^2 (1 + \tan^2\alpha)} \quad (2.28)$$

After some simple rearranging, we arrive at the following long wave equation for  $k_x$  at the boundary:

$$\Rightarrow R^2 (1 + \tan^2\alpha) k_x^2 + \frac{\beta R^2}{\omega} k_x + 1 = 0 \quad (2.29)$$

$$\Rightarrow \left( \frac{1}{\cos^2\alpha} \right) k_x^2 + \frac{\beta}{\omega} k_x + \frac{1}{R^2} = 0 \quad (2.30)$$

$$\Rightarrow k_x^{long} = -\frac{\beta \cos^2\alpha}{2\omega} + \frac{\cos^2\alpha}{2} \sqrt{\left( \frac{\beta}{\omega} \right)^2 - \frac{4}{R^2 \cos^2\alpha}} \quad (2.31)$$

We can then calculate  $k_y$  using equation (2.27). The maximum frequency and critical latitude are now dependent on the angle of the coastline and can be written as follows:

$$\omega_{max} = \frac{c_0 \cos\alpha}{2y} \quad (2.32)$$

$$y_c = \frac{c_0 \cos \alpha}{2\omega} \quad (2.33)$$

We can now also define a critical coastline angle  $\alpha_c$ . The critical coastline angle represents the maximum angle from a north-south orientated boundary for which Rossby waves can still propagate for a given latitude and frequency:

$$\alpha_c = \cos^{-1} \left( \frac{2\omega y}{c_0} \right) \quad (2.34)$$

Having altered the model to properly account for variable coastline geometry, we can now examine the effect that this has on the ray paths. First we will consider a straight coastline, orientated at an angle of  $\alpha = \pm 45^\circ$  from the meridian. The result of this is shown in Figure (2.5).

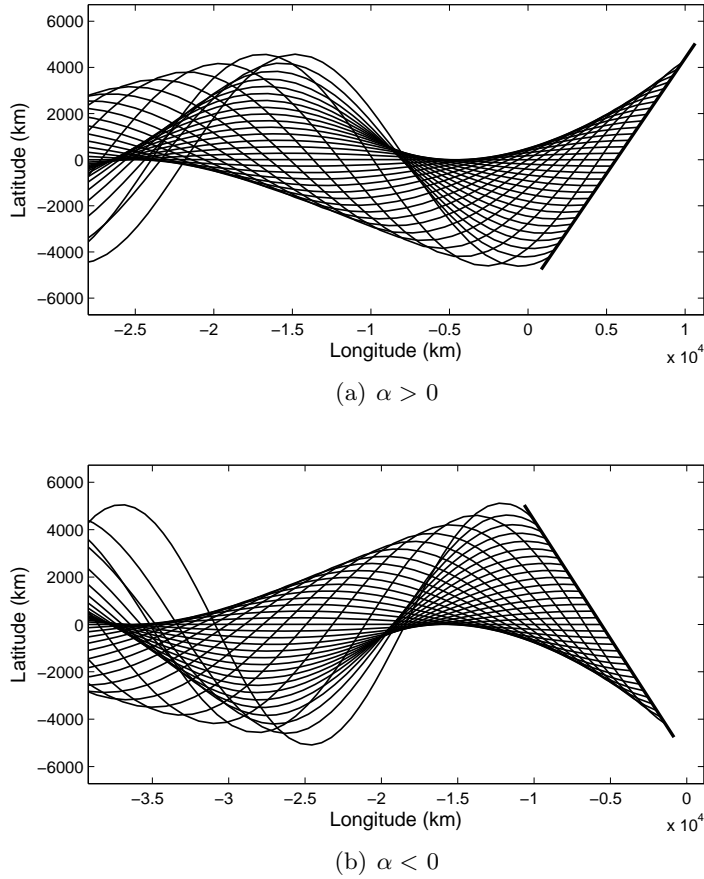


Figure 2.5: Rays from a sloping eastern boundary.

If we initially look at the north east orientated boundary, it is clear that one effect of

introducing a variable meridional wavenumber along the boundary is that the ray paths are now initially orientated slightly towards the south as they leave the coastline. In addition, the angle of the boundary means that the caustic in the northern hemisphere is developing nearer to the equator, and the energy focus described by Schopf et al. (1981) is located slightly north of the equator. Schopf et al. (1981) defines an equation to specify the  $(x,y)$  position of the energy focus for a straight coastline orientated at some angle  $\alpha$  from the meridian:

$$x = -\frac{\pi c_0}{4\omega} - \frac{3c_0}{2\pi\omega} \sin^2 \alpha \quad (2.35)$$

$$y = -\frac{c_0}{\pi^2 \omega} \sin^3 \alpha \quad (2.36)$$

Also to be considered is the effect of the angle of the coastline on the critical latitude. For a north-south orientated coastline the critical latitude was calculated to be approximately  $y_c = 6500\text{km}$ . For a straight coastline orientated at an angle of  $\alpha = 45^\circ$  from the meridian, it can be shown from equation (2.33) that the critical latitude is approximately  $y_c = 4600\text{km}$ . This is consistent with the extent shown in Figure (2.5). Our final consideration is the fact that ray paths for a north-west orientated boundary are simply a reflection about the equator of the paths from the north-east orientated boundary.

We will now examine ray paths propagating on a more local scale from a slowly varying coastline as opposed to a simple straight boundary. Figure (2.6) shows ray solutions from a section of the South Pacific eastern coastline. The most prominent effect of the variable coastline on the ray paths is the presence of convergence and divergence of ray paths depending on the local coastline shape. There are several consequences this can have on the propagation of Rossby waves. Areas where the ray paths diverge are likely to be areas with less energy and thus weaker Rossby wave activity. Areas of ray convergence are likely to be areas of energy focus, with enhanced variability associated with the Rossby waves. The third possibility is that rays may converge to the point of crossing, in which case the coastline shape can cause caustic formation within the interior of the ray envelope.

Finally we consider the effect of introducing a variable meridional wavenumber along the Atlantic and Pacific coastlines by solving for the ray trajectories across the entire ocean basins. The results are shown in Figure (2.7) below. It is immediately obvious that the solutions are not as neat and tidy as those shown previously, this being a result of the frequent variations in the coastal geometry. There are regions of ray divergence and convergence, and rays propagating from the North Atlantic coastline are particularly chaotic due to the high variability in  $\alpha$  over a relatively small distance.

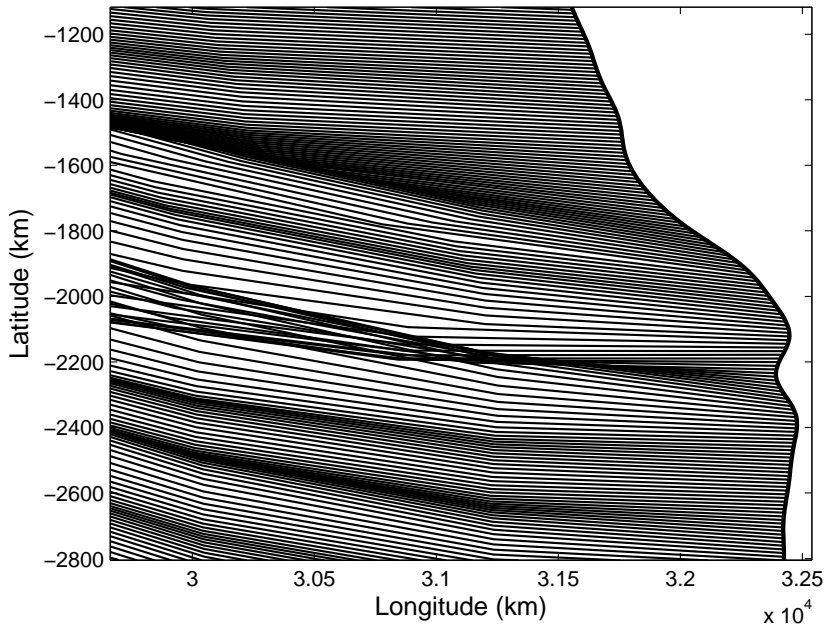


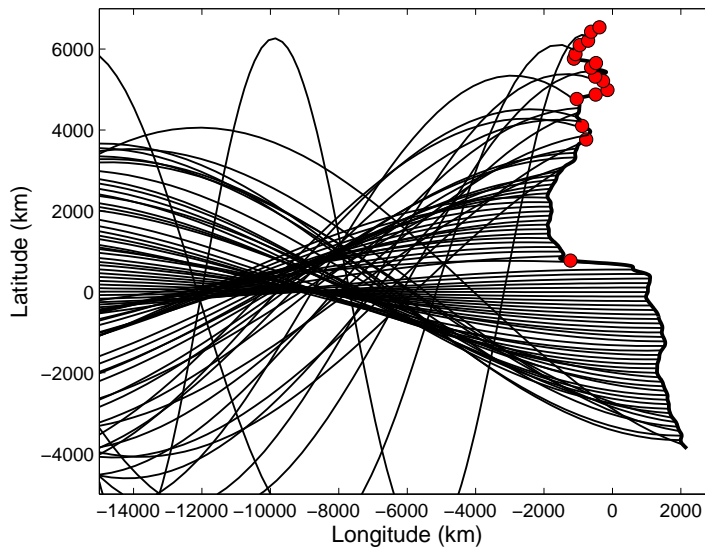
Figure 2.6: Rays propagating on a local scale from the south-eastern Pacific coastline.

The critical latitude  $y_c$  is dependent on the angular frequency  $\omega$ , the gravity-wave phase speed  $c_0$  and the coastline angle  $\alpha$ . However as we have taken  $\omega$  and  $c_0$  to be constant, while  $\alpha$  varies along the coastline, the critical latitude is now a function of  $\alpha$  and also varies along the coastline. It is clear that the more the coastline leans in the east-west direction the lower the critical latitude, where a totally east-west coastline prevents any wave propagation taking place at all.

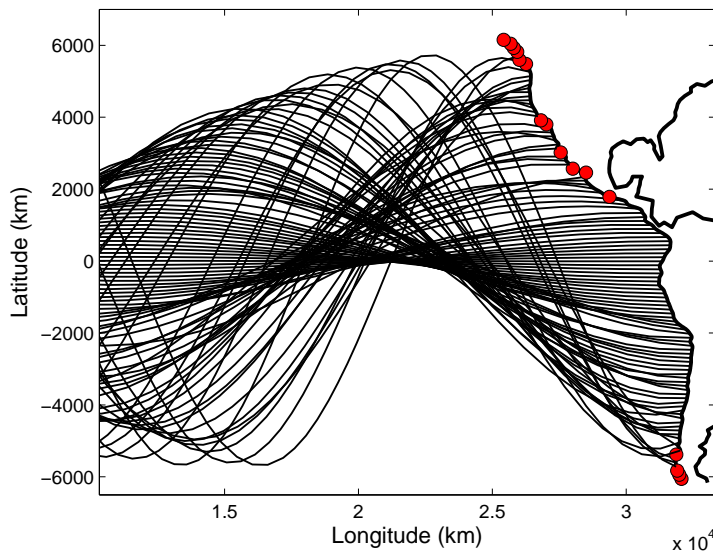
The effect of  $\alpha$  on the critical latitude is most significant in the higher latitudes. This is because for  $\alpha \neq 0$ ,  $y_c$  will be reduced, and in the higher latitudes this is more likely to result in the zonal wavenumber becoming complex at the boundary. Of course, this can occur at any latitude for a sufficiently tilted coastline. The overall result of this is that there are areas along the eastern boundary equatorwards of the actual critical latitude (beyond which no Rossby waves propagate from the boundary), from which Rossby waves cannot propagate due to the slope of the coastline. This is frequently the case in the North Pacific and the North Atlantic although there are some examples of this closer to the equator such as on the West coast of Africa.

Sections of the coastline with a complex initial zonal wavenumber will be marked in red

in figures from this point on. In general it has been shown that coastal geometry is an important factor in determining the energy distribution associated with oceanic Rossby waves.



(a) Atlantic Ray Paths



(b) Pacific Ray Paths

Figure 2.7: Ray paths with variable meridional wavenumber at the boundary for (a) Atlantic Ocean and (b) Pacific Ocean. Red circles indicate latitudes beyond the critical latitude or at which no Rossby wave propagation occurs due to the angle of the coastline.

### 2.1.8 Variable $c_0$

Up to this point, we have made the assumption that the gravity-wave phase speed has a zonally and meridionally constant value of  $c_0 = 2.6\text{ms}^{-1}$ . In reality, the phase speed of Rossby waves is not constant and changes with both latitude and longitude. The phase speed is an important factor both in terms of determining the critical latitude, and in determining the shape of the rays themselves. It can therefore be deduced that introducing a variable phase speed may be a good way of improving the model.

Chelton et al. (1998) concentrated on computing global climatologies of the first baroclinic gravity-wave phase speed and Rossby radius of deformation every  $1^\circ$  of latitude and longitude. Subsequently, one option for introducing a variable phase speed into our model would be to use the two dimensional Matlab interpolation function so that as we integrate for each ray solution, the group velocity of the ray is calculated using the interpolated phase speed value specified according to its location in the oceanic basin.

Another, perhaps more simple option, would be to use an analytical phase speed function for the Atlantic and Pacific oceans such that it closely fits the observed data. Having considered the observational data, the initial analytical function derived for the Atlantic and Pacific phase speeds is as follows:

$$c_0(y) = A + B\cos\left(\frac{2y}{a} + C\pi\right) + D\cos\left(\frac{6y}{a} + \pi\right); \quad (2.37)$$

where the parameters  $A$ ,  $B$  and  $D$  have the same dimensions as  $c_0$  ( $\text{ms}^{-1}$ ) and  $C$  is a non-dimensional parameter. As we are using a non-constant phase speed, we must redefine equation (2.14). In general we can write equation (2.14) in autonomous form as:

$$\frac{dk_y}{dx} = \frac{(R^2)_y k_x}{R^2 [1 + R^2 (k_y^2 - k_x^2)]} \quad (2.38)$$

where  $(R^2)_y$  is the rate of change of the Rossby radius of deformation with respect to  $y$  and  $R$  depends on the analytical phase speed function  $c_0(y)$ .

For the global zonal mean, latitudinal distribution, we choose parameter values of  $A = 2\text{ms}^{-1}$ ,  $B = 1\text{ms}^{-1}$ ,  $C = 0$  and  $D = 0.3\text{ms}^{-1}$ . Figure (2.8) is a comparison of the resulting phase speed function and the observed global mean phase speeds. Mean latitudinal phase speed distributions were also calculated from the Chelton et al. (1998) dataset, between  $70^\circ\text{W}$  and  $20^\circ\text{E}$  for the Atlantic ocean and between  $160^\circ\text{E}$  and  $70^\circ\text{W}$  for the Pacific ocean. The values of the  $A$ ,  $B$ ,  $C$  and  $D$  parameters in equation (2.35) were then altered to more

closely fit the observed phase speeds in the particular ocean basin. The results of these alterations are shown in Figure (2.9).

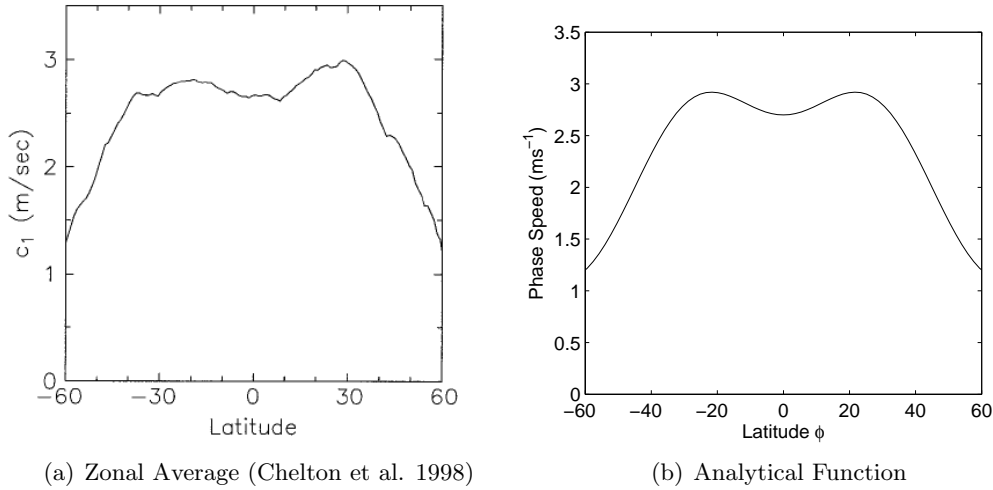


Figure 2.8: (a) The global zonally averaged first order baroclinic mode gravity-wave phase speed obtained by Chelton et al. (1998). (b) The latitudinal variation in gravity-wave phase speed provided by the derived function specified by equation (2.37).

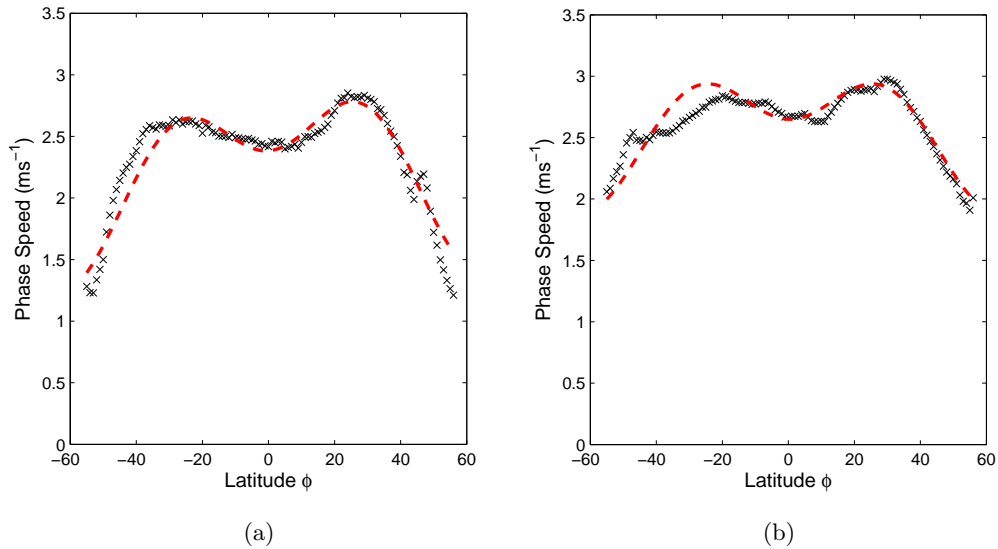


Figure 2.9: A comparison of the zonally averaged phase speed for (a) the Atlantic Ocean and (b) the Pacific Ocean, with the analytical function using the specified parameters for each respective ocean basin.

The parameters for the Atlantic ocean were chosen to be  $A = 2\text{ms}^{-1}$ ,  $B = 0.7\text{ms}^{-1}$ ,  $C = -0.02$  and  $D = 0.31\text{ms}^{-1}$ . For the Pacific ocean, the parameter values are  $A = 2.4\text{ms}^{-1}$ ,  $B = 0.5\text{ms}^{-1}$ ,  $C = 0$  and  $D = 0.25\text{ms}^{-1}$ . It can be seen that the zonally averaged phase speeds in the Pacific are generally faster than the Atlantic, however there are greater meridional variations in the phase speed in the Atlantic, particularly towards to the mid-latitudes.

In an attempt to improve the analytical function further, we could also take into account longitudinal variations in phase speed. Figure (2.10) shows the change in meridionally averaged phase speeds beginning from the eastern boundaries of the Atlantic and Pacific oceans respectively.

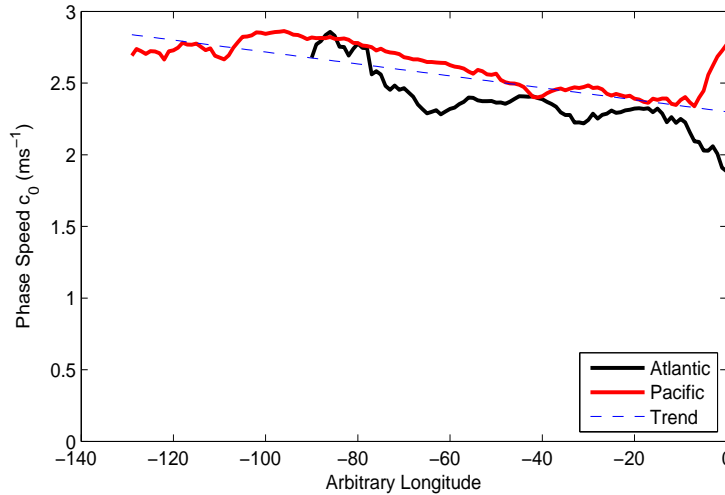


Figure 2.10: Meridionally averaged phase speeds for the Atlantic and Pacific oceans where  $0^\circ$  longitude represents the eastern coastline.

The first thing to note is that in general, the longitudinal variations in phase speed do not seem to be as significant as the latitudinal variations. The phase speeds also seem to increase from east to west, possibly due to topographic influences (Killworth and Blundell, 1999 and Tailleux and McWilliams, 2002) or the presence of a background mean flow (Killworth et al., 1997). In the Pacific Ocean, the longitudinal change in phase speed is on average, an increase from East to West by approximately  $0.5\text{ms}^{-1}$  whereas in the Atlantic there is an increase of around  $0.7\text{ms}^{-1}$ .

We could introduce a simple additional term such that the phase speed increases linearly westward across the ocean basin. The resulting analytical function would be as follows:

$$c_0(x, y) = A + B \cos\left(\frac{2y}{a}\right) + C \cos\left(\frac{6y}{a} + D\pi\right) + \frac{Ex}{a}; \quad (2.39)$$

where the additional parameter  $E$  has the dimensions of phase speed ( $\text{ms}^{-1}$ ) and determines how fast the phase speed increases from East to West. Introducing an  $x$ -dependent phase speed function means that the zonal wavenumber  $k_x$  is no longer conserved along each ray. We are therefore required to rewrite equation (2.13) which in general takes the following autonomous form:

$$\frac{dk_x}{dx} = \frac{(R^2)_x k_x}{R^2 [1 + R^2 (k_y^2 - k_x^2)]} \quad (2.40)$$

where  $(R^2)_x$  is the rate of change of the Rossby radius of deformation with respect to  $x$  and  $R$  depends on the analytical phase speed function  $c_0(x, y)$ .

Figures (2.11) and (2.12) show the relative errors associated with the assumption of constant phase speed and using the  $y$ -dependent analytical function for  $c_0$  in the Atlantic and Pacific oceans respectively. Figure (2.13) shows the error associated with the two-dimensional function for  $c_0$  in the Pacific Ocean only. The errors were calculated by making a comparison with the observed phase speeds from the Chelton et al. (1998) dataset. The  $y$ -dependent function is a dramatic improvement for  $c_0$  in the Atlantic Ocean, particularly in the mid-latitudes. There are some underestimates and overestimates  $>0.3\text{ms}^{-1}$  in the upper hemisphere, particularly along the northern part of the coastline which may be significant for accurately determining the critical latitude.

The assumption of constant  $c_0$  for the Pacific Ocean produces significant errors in the western part of the basin and in the high latitudes. The  $y$ -dependent function is a huge improvement in these areas but there is a general underestimate  $>0.3\text{ms}^{-1}$  along the eastern coastline. The two-dimensional function for the Pacific clearly produces a phase speed distribution that more closely matches the observed Rossby wave phase speeds as errors are generally less than  $0.3\text{ms}^{-1}$  across the entire ocean basin.

It is clear that the analytical functions provide a better estimate for the overall gravity-wave speed distribution. There are some significant errors along the eastern boundaries however, and this will have an effect on the critical latitude  $y_c$ , which becomes a function of  $\alpha$  and  $c_0$  when the variable  $c_0$  is introduced. Ideally we would like to interpolate observed values of  $c_0$  from the Chelton et al. (1998) dataset, but this proved somewhat difficult to implement. The two-dimensional analytical function is the best alternative, however having attempted to include it within the model, it proved problematic to test that the

distribution of  $c_0$  values specified by the function was correct. For simplicity, and so that we can be certain that the analytical function specifies the correct phase speed distribution for each ocean basin, we will use the  $y$ -dependent function given by equation (2.37), which provides a middle-ground in terms of accuracy. In further work, interpolation of the dataset or the two-dimensional phase speed function should be implemented for more realistic results.

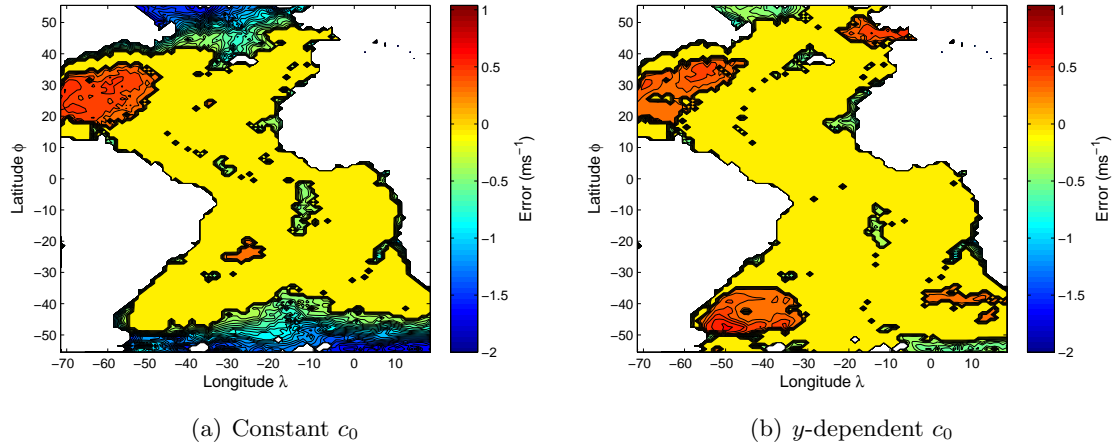


Figure 2.11: Error between the observed phase speeds and (a) constant  $c_0$  (b) analytic function  $c_0(y)$  in the Atlantic Ocean. Phase speed errors  $< 0.3\text{ms}^{-1}$  are shown in yellow.

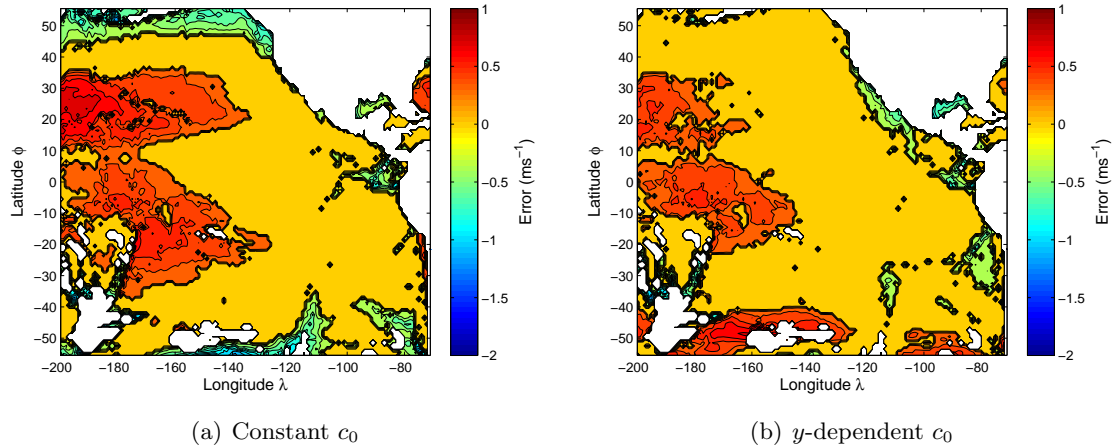


Figure 2.12: Error between the observed phase speeds and (a) constant  $c_0$  (b) analytic function  $c_0(y)$  in the Pacific Ocean. Phase speed errors  $< 0.3\text{ms}^{-1}$  are shown in yellow.

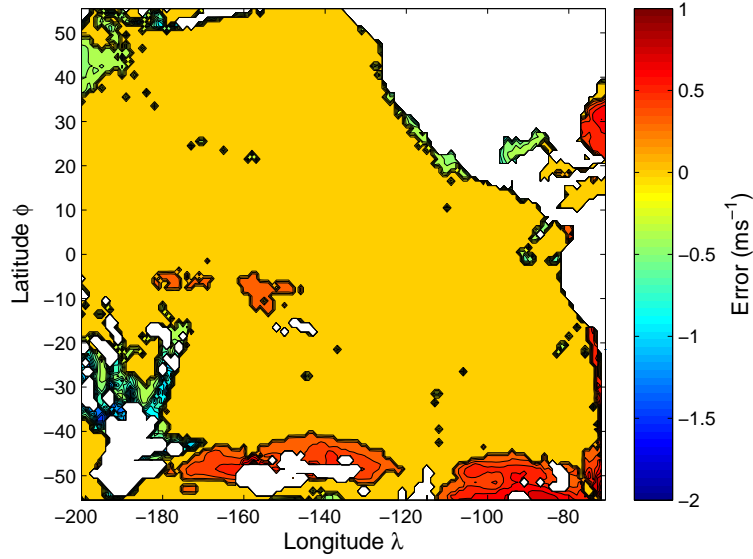
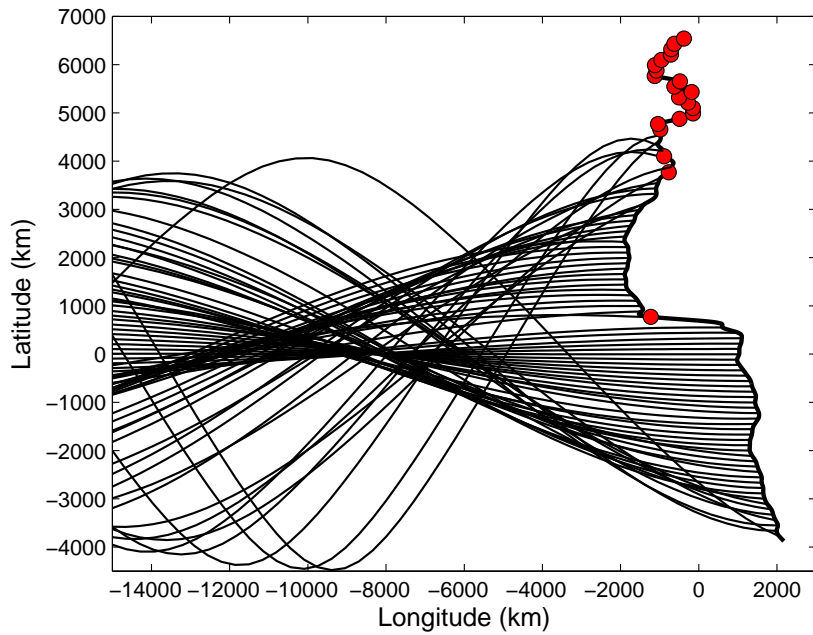
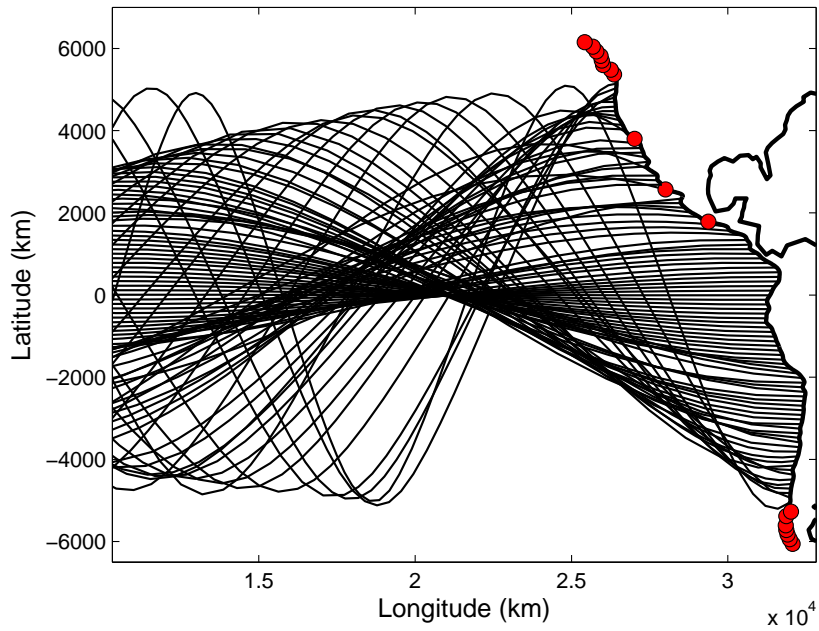


Figure 2.13: Error between the observed phase speeds and the analytic function  $c_0(x, y)$ . Phase speed errors  $< 0.3 \text{ms}^{-1}$  are shown in yellow.

After some lengthy calculations, the ray equations were re-derived to account for the variable phase speed. It was however somewhat difficult to simplify the equation for  $k_y$  such that it is included in the appendix only (Appendix (1.5.1)). The resulting ray solutions are shown in Figure (2.14). An obvious effect of introducing the variable phase speed is the change in critical latitude and thus the latitudinal extent along the eastern boundary from which Rossby waves can propagate. In general there is a significant reduction by several degrees of the critical latitude  $y_c$  for both the Atlantic and Pacific ocean basins. This is a result of there being values of  $c_0$  that are less than  $2.6 \text{ms}^{-1}$  in the mid-latitudes. The western extent of the ray solutions, particularly in the Pacific, also seems to have reduced slightly in the higher latitudes due to the reduction in  $c_0$ . The value of  $c_0$  is therefore important in determining both the zonal and meridional extent of Rossby wave propagation in the ocean and also the general shape of the ray envelope.



(a) Atlantic Ray Paths



(b) Pacific Ray Paths

Figure 2.14: Ray paths with variable meridional wavenumber at the boundary and variable  $c_0$  for (a) Atlantic Ocean and (b) Pacific Ocean. Red circles indicate latitudes beyond the critical latitude or at which no Rossby wave propagation occurs due to the angle of the coastline.

## 2.2 Spherical Polar Coordinates

So far we have used the  $\beta$ -plane approximation in the derivation of our ray equations. We now extend the theory to account for the curvature of the Earth by using spherical geometry. The transformation from cartesian geometry is relatively simple. Rather than assuming that the  $\beta$ -parameter is constant and that the coriolis parameter  $f$  varies linearly, we use their full definitions:

$$f = 2\Omega \sin\phi \quad (2.41)$$

$$\beta = \frac{2\Omega \cos\phi}{a} \quad (2.42)$$

such that they both retain their latitudinal variations and where  $\Omega$  is the rate of Earth's rotation and  $a$  is Earth's radius. As in Killworth and Blundell (2003), we also express the cartesian wavenumbers  $k_x$  and  $k_y$  in terms of the angular wavenumbers  $k_\lambda$  and  $k_\phi$ :

$$k_x = \frac{k_\lambda}{a \cos\phi} \quad (2.43)$$

$$k_y = \frac{k_\phi}{a} \quad (2.44)$$

where  $\lambda$  and  $\phi$  are longitude and latitude respectively.

### 2.2.1 Dispersion Relationship

Using the angular wavenumber terms given by equations (2.43) and (2.44) we can rewrite the dispersion relationship in spherical polar coordinates:

$$\omega = \frac{-\beta R^2 a \cos\phi k_\lambda}{a^2 \cos^2\phi + R^2 (k_\lambda^2 + \cos^2\phi k_\phi^2)} \quad (2.45)$$

where  $\omega$  is now a function of  $\phi$  and the angular wavenumbers  $k_\lambda$  and  $k_\phi$ .

### 2.2.2 Ray Equations

We derive the ray equations in spherical polar coordinates as for cartesian coordinates, however this time we systematically differentiate the dispersion relationship with respect to  $\lambda$ ,  $\phi$  and the angular wavenumber terms. After some careful calculations, it can be shown that for a constant gravity-wave phase speed  $c_0$ , the ray equations are:

$$\frac{d\lambda}{dt} = c_{g\lambda} = \frac{\partial\omega}{\partial k_\lambda} = -\frac{\beta R^2 a \cos^3\phi \left[ a^2 + R^2 \left( k_\phi^2 - k_\lambda^2 / \cos^2\phi \right) \right]}{\left[ a^2 \cos^2\phi + R^2 \left( k_\lambda^2 + \cos^2\phi k_\phi^2 \right) \right]^2} \quad (2.46)$$

$$\frac{d\phi}{dt} = c_{g\phi} = \frac{\partial\omega}{\partial k_\phi} = \frac{2\beta R^4 a \cos^3 \phi k_\lambda k_\phi}{\left[ a^2 \cos^2 \phi + R^2 \left( k_\lambda^2 + \cos^2 \phi k_\phi^2 \right) \right]^2} \quad (2.47)$$

$$\frac{dk_\lambda}{dt} = -\frac{\partial\omega}{\partial \lambda} = 0 \quad (2.48)$$

$$\frac{dk_\phi}{dt} = -\frac{\partial\omega}{\partial \phi} = -\frac{2\beta R^2 a k_\lambda \left( R^2 \sin^2 \phi k_\lambda^2 + a^2 \cos^4 \phi \right)}{\sin \phi \left[ a^2 \cos^2 \phi + R^2 \left( k_\lambda^2 + \cos^2 \phi k_\phi^2 \right) \right]^2} \quad (2.49)$$

It can once more be shown from equation (2.46) that in order for the group velocity to be negative in the  $\lambda$ -direction, the following condition must be satisfied:

$$a^2 + R^2 \left( k_\phi^2 - k_\lambda^2 / \cos^2 \phi \right) > 0 \quad (2.50)$$

where  $\beta = 2\Omega \cos \phi / a$  and  $\cos \phi > 0$ . This condition is equivalent to:

$$k_\lambda^2 < \cos^2 \phi \left( \frac{a^2}{R^2} + k_\phi^2 \right) \quad (2.51)$$

which corresponds to long wave solutions as required.

### 2.2.3 Autonomous Equations

We have shown that for long waves, the group velocity in the  $\lambda$  direction is always negative, i.e.  $c_{g\lambda} < 0$ . For the same reasons stated in the section on cartesian coordinates, and as we know it to be valid since  $c_{g\lambda} < 0$ , we will therefore reduce our system of ordinary differential equations to an autonomous one. From equation (2.46):

$$\frac{d\lambda}{dt} = c_{g\lambda} \quad (2.52)$$

and we can therefore write:

$$dt = \frac{d\lambda}{c_{g\lambda}} \quad (2.53)$$

Using this, we can rewrite our equations for  $\phi_t$  and  $(k_\phi)_t$  as follows:

$$\frac{d\phi}{d\lambda} = \frac{c_{g\phi}}{c_{g\lambda}} \quad (2.54)$$

$$\frac{dk_\phi}{d\lambda} = \frac{1}{c_{g\lambda}} \frac{dk_\phi}{dt} \quad (2.55)$$

Thus our autonomous system of differential equations is given as:

$$\frac{d\phi}{d\lambda} = \frac{-2R^2 k_\lambda k_\phi}{\left[ a^2 + R^2 \left( k_\phi^2 - k_\lambda^2 / \cos^2 \phi \right) \right]} \quad (2.56)$$

$$\frac{dk_\lambda}{d\lambda} = 0 \quad (2.57)$$

$$\frac{dk_\phi}{d\lambda} = \frac{2k_\lambda \left( R^2 \sin^2 \phi k_\lambda^2 + a^2 \cos^4 \phi \right)}{\sin \phi \cos^3 \phi \left[ a^2 + R^2 \left( k_\phi^2 - k_\lambda^2 / \cos^2 \phi \right) \right]} \quad (2.58)$$

#### 2.2.4 Fixed $\omega$ Solution

We will begin by integrating for a straight north-south eastern boundary, in which case we can assume a boundary condition of constant phase  $S$ . This implies that  $k_\phi = 0$  along the boundary and we can therefore initially write the dispersion relationship as:

$$\omega = \frac{-\beta R^2 a \cos \phi k_\lambda}{a^2 \cos^2 \phi + R^2 k_\lambda^2} \quad (2.59)$$

This can be rearranged so that we have a quadratic equation to solve for the initial value of  $k_\lambda$  along the eastern boundary:

$$R^2 k_\lambda^2 + \frac{\beta R^2 a \cos \phi}{\omega} k_\lambda + a^2 \cos^2 \phi = 0 \quad (2.60)$$

The solution of this equation that corresponds to long waves is as follows:

$$k_\lambda^{long} = \frac{a \cos \phi \left( -\beta R + \sqrt{\beta^2 R^2 - 4\omega^2} \right)}{2R\omega} \quad (2.61)$$

From equation (2.57), it is shown that  $k_\lambda$  is constant when integrating with respect to  $\lambda$ , and thus the value of  $k_\lambda$  specified by equation (2.61) is conserved along each ray trajectory.

#### 2.2.5 Critical Latitude

It is clear that to avoid a complex solution for the zonal wavenumber, the following condition must be satisfied:

$$\beta^2 R^2 - 4\omega^2 > 0 \quad (2.62)$$

Keeping in mind that  $\beta$  and  $f$  now retain their latitudinal variations this is equivalent to:

$$\omega < \frac{\beta c_0}{2f} = \frac{c_0 \cos \phi}{2a \sin \phi} \quad (2.63)$$

From this we can calculate the maximum frequency for which Rossby waves can propagate freely from the eastern boundary:

$$\omega_{max} = \frac{c_0}{2a \tan \phi} \quad (2.64)$$

To determine the critical latitude in spherical polar coordinates, we simply rewrite equation (2.63):

$$\Rightarrow f < \frac{\beta c_0}{2\omega} \quad (2.65)$$

The critical latitude is therefore given by:

$$\phi_c = \tan^{-1} \left( \frac{c_0}{2a\omega} \right) \quad (2.66)$$

Using a constant gravity-wave phase speed of  $c_0 = 2.6 \text{ms}^{-1}$  and a fixed annual frequency, it can be shown that the critical latitude for a north-south orientated straight coastline is  $\phi_c \approx 45.7^\circ$ . This is illustrated in Figure (2.15).

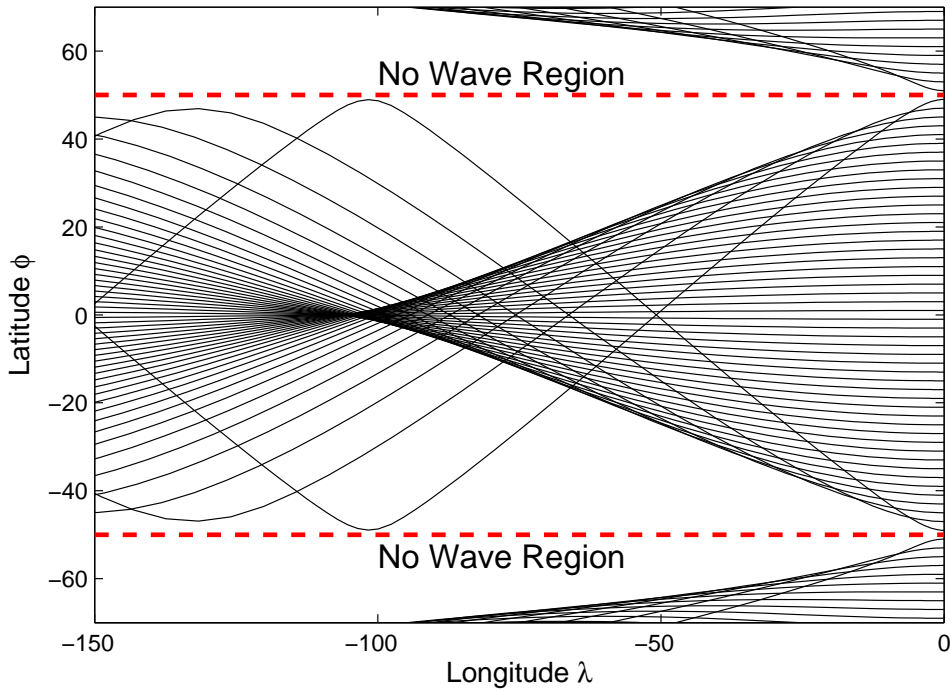


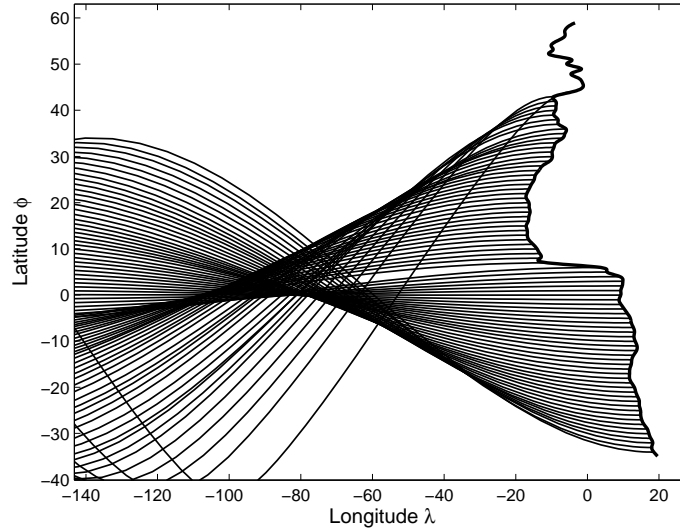
Figure 2.15: Ray paths in spherical polar coordinates for a straight, north-south orientated boundary with a zero initial angular meridional wavenumber

If we consider that the critical latitude in cartesian coordinates was roughly 6525km and

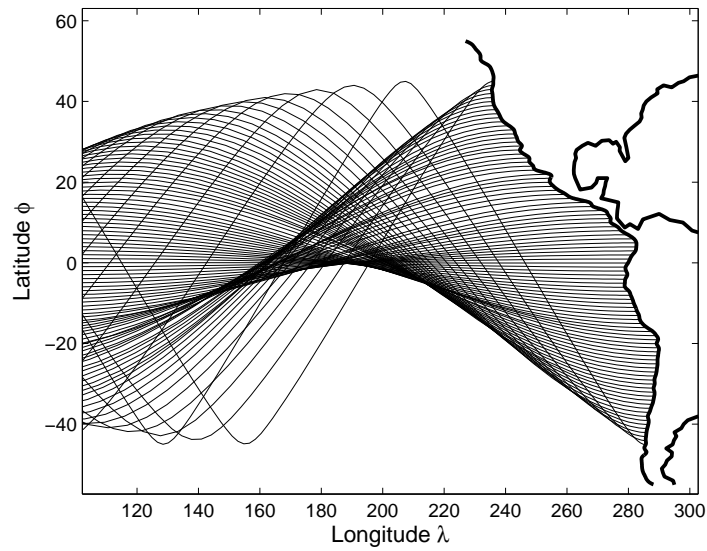
use a conversion ratio of 112km per degree, then the critical latitude for the cartesian coordinate solution in degrees is approximately  $58.3^\circ$ . It is therefore clear that converting to spherical geometry has a direct effect on the extent of the critical latitude when considering a straight north-south boundary. In addition, although still symmetric about the equator, the ray envelope has a slightly different shape. This is a result of allowing the  $\beta$  and  $f$  parameters to retain their latitudinal variations.

### 2.2.6 Realistic Coastlines

We now introduce realistic coastlines to the model, illustrated in Figure (2.16).



(a) Atlantic Ray Paths



(b) Pacific Ray Paths

Figure 2.16: Ray paths for (a) the Atlantic Ocean and (b) the Pacific Ocean with a zero meridional wavenumber at boundary.

### 2.2.7 Variable Meridional Wavenumber

For a non-straight boundary, we can no longer assume an initial value of  $k_\phi = 0$ . Using equation (2.27) and converting the cartesian wavenumbers into angular wavenumbers yields the following boundary condition:

$$k_\phi = -\frac{k_\lambda}{\cos\phi} \frac{d\lambda_e}{dy} \quad (2.67)$$

where  $d\lambda_e/d\phi = -\tan\alpha$ . We must now form a new equation for the zonal wavenumber, before the meridional wavenumber can subsequently be calculated. The dispersion relationship at the eastern boundary becomes:

$$\omega = \frac{-\beta R^2 a \cos\phi k_\lambda}{a^2 \cos^2\phi + R^2 k_\lambda^2 (1 + \tan^2\alpha)} \quad (2.68)$$

$$\Rightarrow \left(\frac{1}{\cos^2\alpha}\right) k_\lambda^2 + \frac{\beta a \cos\phi}{\omega} k_\lambda + \frac{a^2 \cos^2\phi}{R^2} = 0 \quad (2.69)$$

which is simply a quadratic equation for  $k_\lambda$  whose long wave solution is given by:

$$\Rightarrow k_\lambda^{long} = -\frac{\beta a \cos\phi \cos^2\alpha}{2\omega} + \frac{\cos^2\alpha}{2} \sqrt{\left(\frac{\beta a \cos\phi}{\omega}\right)^2 - \left(\frac{2a \cos\phi}{R \cos\alpha}\right)^2} \quad (2.70)$$

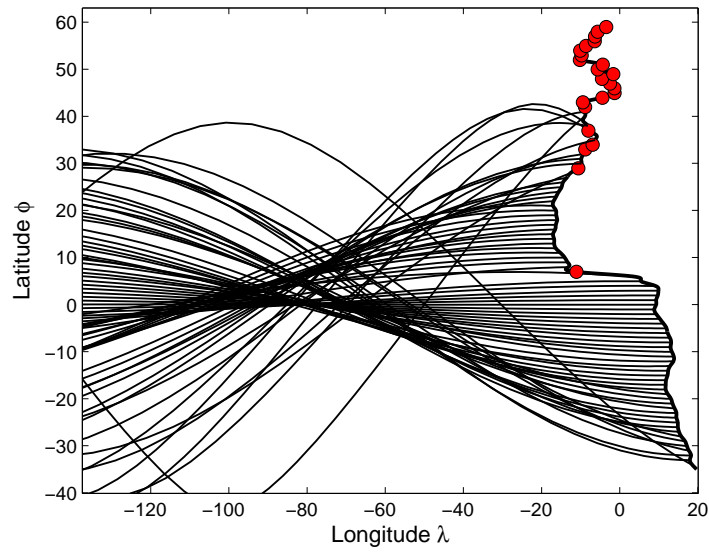
This equation is solved for the initial value of  $k_\lambda$  before  $k_\phi$  is calculated from equation (2.67). As in cartesian coordinates we can now redefine the maximum frequency, critical latitude and critical coastline angle in spherical polar coordinates:

$$\omega_{max} = \frac{c_0 \cos\alpha}{2a \tan\phi} \quad (2.71)$$

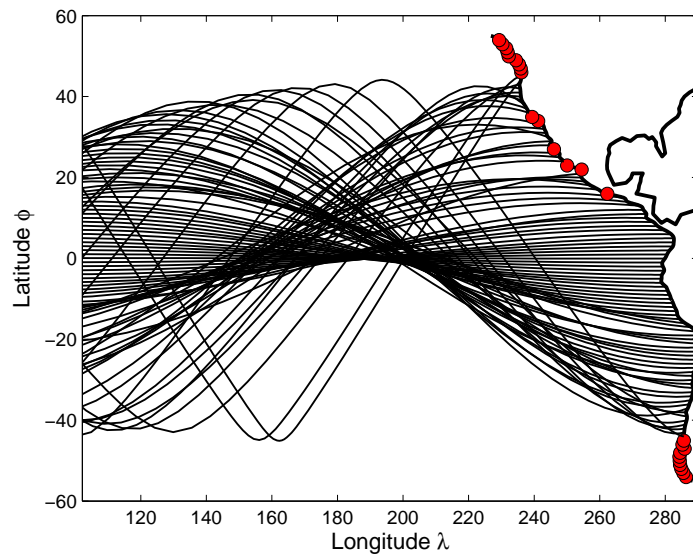
$$\phi_c = \tan^{-1} \left( \frac{c_0 \cos\alpha}{2a\omega} \right) \quad (2.72)$$

$$\alpha_c = \cos^{-1} \left( \frac{2a\omega \tan\phi}{c_0} \right) \quad (2.73)$$

The effect of introducing a variable meridional wavenumber can be seen in Figure (2.17). The overall impact is similar to the  $\beta$ -plane solution. The angle from which the ray propagates from the coastline now depends on the angle of the coastline relative to the meridian. Thus for  $\alpha > 0$ , rays leave the coastline initially heading southwards, and for  $\alpha < 0$ , rays leave the coastline initially heading northwards. There are therefore regions of ray divergence and convergence, particularly where the coastline varies significantly over a small distance. The critical latitudes are similar those in the final cartesian coordinate solution but the western extent of the rays in the mid-latitudes seems to be greater overall.



(a) Atlantic Ray Paths



(b) Pacific Ray Paths

Figure 2.17: Ray paths with variable meridional wavenumber at the boundary and constant gravity-wave phase speed  $c_0$  in spherical polar coordinates for (a) the Atlantic Ocean and (b) the Pacific Ocean. Red circles indicate latitudes beyond the critical latitude or at which no Rossby wave propagation occurs due to the angle of the coastline.

### 2.2.8 Variable $c_0$

The last step to achieve the final result in spherical polar coordinates is to remove the assumption that the gravity-wave phase speed is constant. Rather than using  $c_0 = 2.6\text{ms}^{-1}$ , we will once more use the phase speed function specified by equation (2.37). In spherical polar coordinates this is equivalent to:

$$c_0(\phi) = A + B\cos(2\phi + C\pi) + D\cos(6\phi + \pi); \quad (2.74)$$

since  $\phi = y/a$ . Re-deriving the ray equations becomes a little more tedious due to the additional  $\phi$  dependent terms, but the general autonomous form of the equation for  $k_\phi$  can be written:

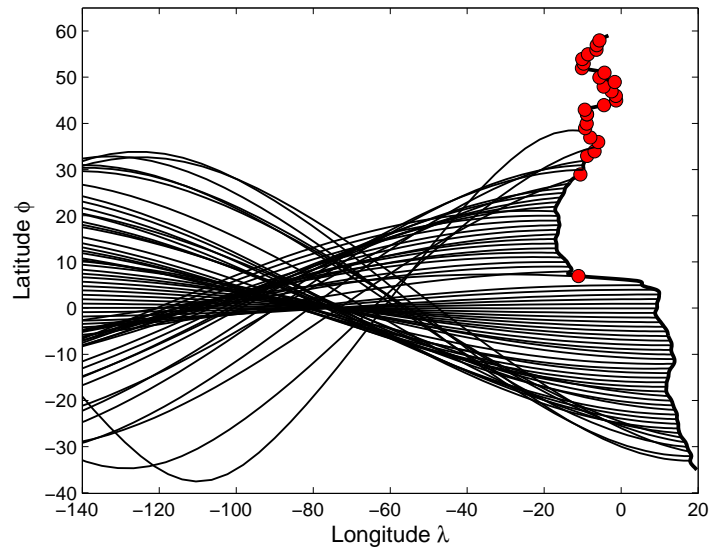
$$\frac{dk_\phi}{d\lambda} = \frac{1}{c_{g\lambda}} \left[ \frac{\partial\omega}{\partial R^2} \frac{\partial R^2}{\partial\phi} + \frac{\partial\omega}{\partial\beta} \frac{\partial\beta}{\partial\phi} + \frac{\partial\omega}{\partial k_x} \frac{\partial k_x}{\partial\phi} \right] \quad (2.75)$$

where  $R = c_0(\phi)/2\Omega \sin\phi$  and  $k_x = k_\lambda/a \cos\phi$ . The full form of this equation is given in Appendix (1.5.2). If we chose to include a gravity-wave phase speed function that is also dependent on  $\lambda$ , then the ray equation for  $k_\lambda$  becomes:

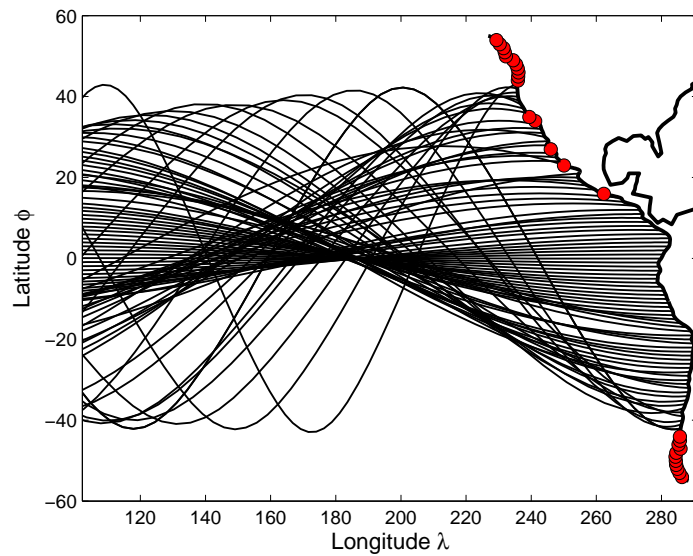
$$\frac{dk_\lambda}{d\lambda} = \frac{1}{c_{g\lambda}} \left[ \frac{\partial\omega}{\partial R^2} \frac{\partial R^2}{\partial\lambda} \right] \quad (2.76)$$

where  $R = c_0(\lambda, \phi)/2\Omega \sin\phi$ . However in the current study, and as for the cartesian coordinate model, we will assume that the gravity-wave speed is variable in  $\phi$  but longitudinally constant.

Figure (2.18) shows the resulting ray solutions for the variable phase speed in spherical polar coordinates. The critical latitude has been marginally reduced as a result of the variable  $c_0$ , while the westward extent of the rays is slightly smaller in the higher latitudes but greater in the lower latitudes. Although the difference is not dramatic, it is certainly easy to discern between the various solutions. This is further confirmation that the phase speed distribution and therefore the change in the Rossby radius of deformation in an ocean basin is important in determining the way in which the wave energy disperses. We can therefore emphasise the significance of using realistic phase speed values when trying to determine the caustics.



(a) Atlantic Ray Paths



(b) Pacific Ray Paths

Figure 2.18: Ray paths with variable meridional wavenumber at the boundary and variable gravity-wave phase speed  $c_0$  in spherical polar coordinates for (a) the Atlantic Ocean and (b) the Pacific Ocean. Red circles indicate latitudes beyond the critical latitude or at which no Rossby wave propagation occurs due to the angle of the coastline.

## 2.3 Caustics

In comparing the final results in cartesian coordinates and spherical polar coordinates (shown by Figures (2.14) and (2.18) respectively), it can be seen that there is very little difference between the two sets of ray solutions. This indicates that the shape of the ray envelope and the caustics is unlikely to be greatly affected by the sphericity of the Earth. The Rossby radius of deformation is the only latitudinal dependent term present in both sets of ray equations due to the variable  $c_0$  and coriolis parameter  $f$ . It can therefore be deduced that the shape of the ray envelope is more a result of the latitudinal variation in the Rossby radius of deformation than due to the sphericity of the Earth. Despite this general similarity, there are some very minor differences that appear as a result of converting to spherical polar coordinates, for example relating to the extent of the critical latitude and the caustics. We can deduce that as the Earth is in fact nearly spherical, that the use of spherical polar coordinates is justified in making for slightly more accurate results.

Having achieved our final result, it is clear that in some areas, the exact location of the caustics is not easy to define visually. This is particularly the case when we integrate for more ray trajectories from the eastern boundary. The initial direction of rays propagating from the eastern boundary is more variable near to the critical latitude due to the enhanced effect of the coastline angle, and this is particularly the case in the northern hemisphere where the angle of the coastline tends to vary more dramatically. This makes the point at which each ray trajectory first crosses with another a little more difficult to determine.

It does not seem that this issue would be significant if smoother coastline variations for the Atlantic and Pacific coastline had been implemented. When the coastline angle changes significantly over a small distance, areas of strong divergence and converge of rays appear. It is when this occurs that problems can arise in determining the caustic. Variations of the eastern coastline geometry and the validity of the WKB theory is brought up as an important issue by Schopf et al. (1981). We must therefore consider the possibility that some sections of the coastline used within the model vary too quickly over too small a distance to be admitted under WKB theory.

While further work would be to calculate the exact position of the caustics numerically, at the current stage, and although somewhat subjective, we should be able to make a reasonable visual determination of the caustics. These are shown in Figures (2.19) and (2.20) for the Atlantic and Pacific Oceans respectively, where the caustic lines are marked

in red. In addition we include the western coastlines to give a better overall picture.

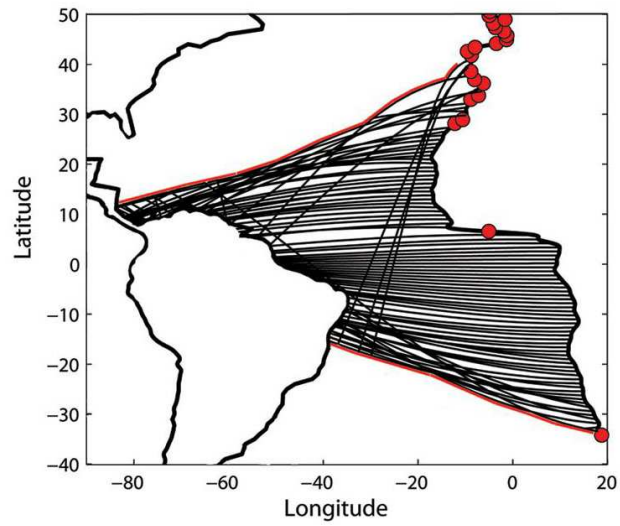


Figure 2.19: Caustics in the Atlantic Ocean

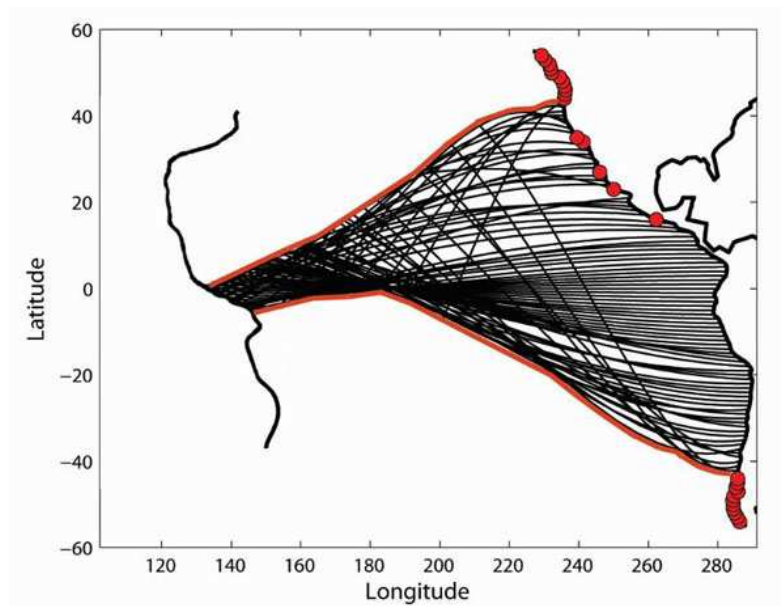


Figure 2.20: Caustics in the Pacific Ocean

For the Atlantic Ocean, the model solution suggests that the critical latitude in the Northern Hemisphere is at approximately  $\phi_c \approx 40^\circ\text{N}$  on the eastern coastline. In the Southern Hemisphere the critical latitude is at the southern tip of Africa at  $\phi_c \approx 35^\circ\text{S}$  where the coastline comes to an end. The poleward extent of the caustic decreases almost linearly westwards (towards the equator) in both hemispheres, until the western coastline is reached. The focus of rays that we have seen in solutions with the western coastline hidden does not occur in the Atlantic because the ocean basin is not wide enough. The caustics instead meet the western coastline at  $13^\circ\text{N}$  just South of the Gulf of Mexico and  $16^\circ\text{S}$  on the East coast of Brazil.

The critical latitude at the eastern coastline of the Pacific Ocean is approximately  $\phi_c \approx 43^\circ\text{N}$  in the Northern Hemisphere and  $\phi_c \approx 42^\circ\text{S}$  in the Southern Hemisphere. The length of the East Pacific coastline from which Rossby waves can propagate is therefore much greater than that of the Atlantic. This is due to faster gravity-wave phase speeds in the Pacific, larger values of  $\alpha$  in the North Atlantic, and particularly due to the fact the tip of South America is almost  $20^\circ$  further South than that of South Africa. The Pacific Ocean basin is also significantly wider than the Atlantic basin. According to the modelled caustics, there is an indication that the majority of boundary-driven Rossby waves from the eastern coastline do not reach the western coastline before being dispersed equatorwards and there is only a very limited region near to the equator where boundary-driven waves from the east can reach the western coastline. There is a sharp focus of energy in the equatorial zone between the longitudes of  $140^\circ$  and  $200^\circ$  which correspond to  $140^\circ\text{E}$  and  $160^\circ\text{W}$  relative to the Greenwich Meridian.

If we once more consider Figure (1.2) from Fu and Qui (2002), we can see that the correlation coefficients between SSH variability in the Pacific Ocean and boundary-driven Rossby waves from the eastern boundary are strongest in the eastern part of the basin. Between  $115^\circ\text{W}$  and  $175^\circ\text{W}$  at  $10^\circ\text{N}$ , there is very little correlation. This corresponds to an area of ray divergence in our theoretical model, which suggests that there may be less energy associated with the boundary-driven waves in this region. Between  $125^\circ\text{E}$  and  $175^\circ\text{W}$ , Figure (1.2) indicates that there is strong correlation between boundary driven waves and SSH variability. This area corresponds to the region in our theoretical model where rays begin to converge, near to the sharp energy focus.

## Chapter 3

# Analysis of Model Output

Many recent studies have used either satellite altimeter data or high resolution ocean models to examine the properties of oceanic Rossby waves. The French CLIPPER model for example, can be used to generate salinity, temperature, SSH and three-dimensional velocity profiles for the Atlantic Ocean and its ability to realistically simulate oceanic Rossby waves has been tested (Lecointre et al. 2008). The model has a resolution of  $1/6^\circ$  on a MERCATOR grid, and 42 geopotential depth levels which are more concentrated near to the surface.

In the model, the ocean surface is forced by realistic atmospheric conditions derived from the ECMWF ERA15 reanalysis dataset. This ensures confidence that waves have been generated by realistic forcing mechanisms such as those that occur over the real oceans. Oceanic Rossby waves are commonly observed by examining SSH anomalies, and it is therefore the SSH data from the model that we shall be considering. The model outputs data every 5 days, and there are 10 years worth of data available from the year 1990 to 2000. We will consider data in the South Atlantic Ocean between  $45^\circ\text{S}$  and  $10^\circ\text{N}$ .

We can therefore attempt to identify the potential location of the caustic in the southern Atlantic Ocean using the model data. Before doing so, some data processing is required so that the relevant data can be isolated. As we have concentrated on modelling caustics for annual frequency Rossby waves, the first step is to apply a filter to the data in order to remove any high frequency anomalies which correspond to processes that operate on a shorter time scale than the Rossby waves under consideration. We can do this by applying a Fast Fourier Transform to the time series for each individual data point  $(x, y)$ . Then by plotting the frequency against the power for each frequency, we can extract the annual frequency and remove any unwanted frequencies. The Inverse Fourier Transform can then be applied so that we are left with the time series of annually varying anomalies. An

example of an unfiltered and filtered time series is given by Figure (3.1), below. Finally, we will remove the zonal mean at each time step in order to prevent any zonal averages from dominating the Rossby wave signals.

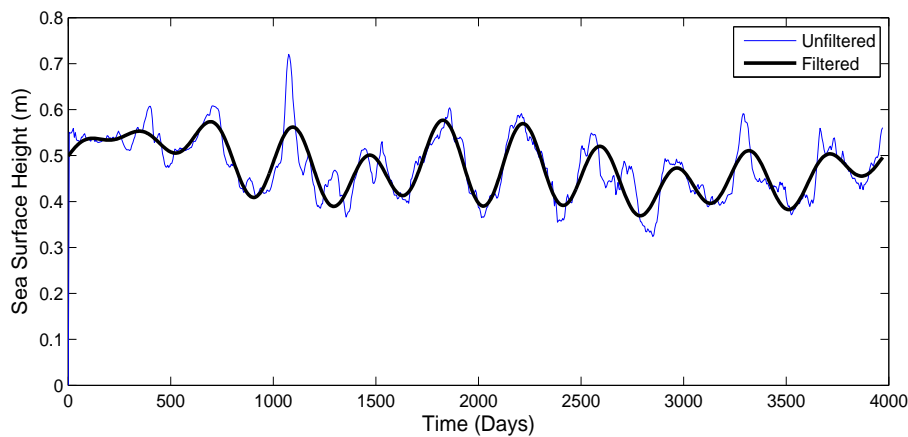


Figure 3.1: Filtered and unfiltered SSH time series.

Having filtered the time series at each data point, the next step is to arrange the data into a longitude-time plot, also known as a Hovmöller diagram. Figures (3.2) and (3.3), below, show examples of an unfiltered and filtered longitude-time plot at  $25^{\circ}\text{S}$ . The Hovmöller diagram gives a dynamical view along zonal sections of the data, and make westward propagating signals easy to identify. The slope of the lines indicating westward propagating signals is inversely proportional to the phase speed of the signal where a more vertically orientated line indicates a more slowly propagating signal.

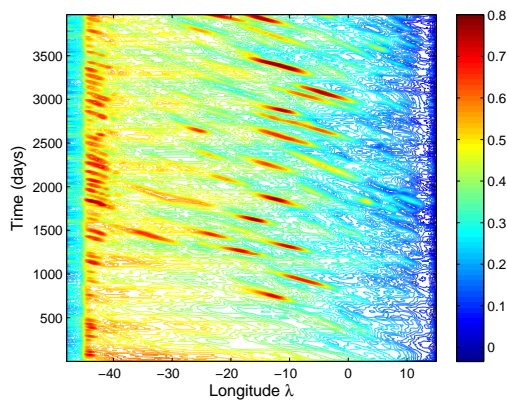


Figure 3.2: Unfiltered time-longitude plot.

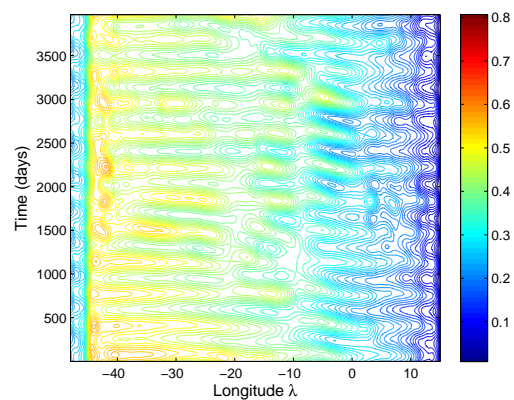


Figure 3.3: Filtered time-longitude plot.

Computational restraints meant that in the current study, we could only examine the longitudinal SSH profiles at 22 equally spaced latitudes, i.e. every  $2.5^\circ$  between  $45^\circ\text{S}$  and  $10^\circ\text{N}$ . Having applied some processing techniques to the data however, we can perform a simple test on the available data in an attempt to detect the caustics by calculating the root mean square variance (RMSV).

First we take the time mean at each point:

$$\bar{\eta}(\lambda, \phi) = \frac{1}{T} \int_0^T \eta(\lambda, \phi, t) dt \quad (3.1)$$

where  $\eta$  is SSH. The RMSV ( $\sigma$ ) is then given by:

$$\sigma(\lambda, \phi) = \frac{1}{T} \int_0^T [\eta(\lambda, \phi, t) - \bar{\eta}(\lambda, \phi)]^2 dt \quad (3.2)$$

Our expectation is that the greatest variance will occur within the region between the caustics in the North and South Hemisphere, as this is where we expect enhanced SSH variability as a result of the annual frequency Rossby waves. Beyond the caustic we expect variability to be relatively small. The result of calculating the RMSV does not necessarily yield the results that we expect.

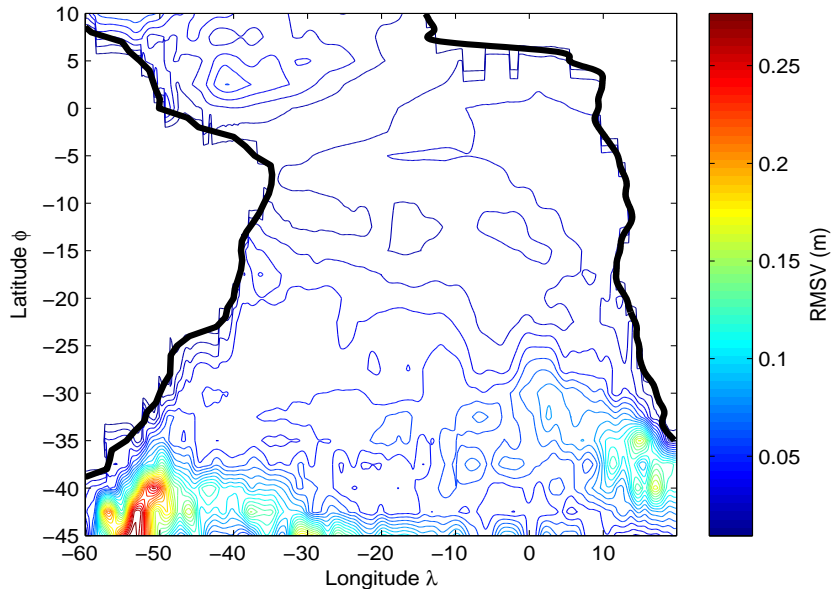


Figure 3.4: Root mean square variability in the South Atlantic Ocean

Figure (3.4) shows the root mean square variability of the filtered SSH data in the South Atlantic Ocean and shows that there is significant variability between  $35^{\circ}\text{S}$  and  $45^{\circ}\text{S}$  in the western part of the basin and between  $33^{\circ}\text{S}$  and  $43^{\circ}\text{S}$  in the eastern part of the basin. The greatest variability occurs in the West and at latitudes South of where we anticipate the modelled caustic to be. There is very little variability further North and this also contradicts our expectations.

Despite this, it can clearly be seen that there are some contours originating from the southern tip of South Africa that go equatorwards and meet the western boundary between  $12^{\circ}\text{S}$ - $16^{\circ}\text{S}$ . The southern hemisphere caustic from our theoretical model also left the southern tip of South Africa and met the western coastline at approximately  $16^{\circ}\text{S}$ . This can be seen in Figure (2.19). There does therefore seem to be some indication of the shape of the caustics derived from our theoretical predictions in the RMSV of the SSH anomalies. This is a good early indicator that such a caustic line is observable in the ocean data and therefore also in the real ocean.

The unexpected pattern of variability shown in Figure (3.4) is likely to be a result of not fully isolating the Rossby wave signal. This indicates that the processing techniques that we have applied are not sufficient to illustrate the regions of high variability and low variability associated purely with the westward propagating Rossby waves. It is also clear that considering SSH profiles only every  $2.5^{\circ}$  of latitude is not sufficient for a proper analysis.

While there is certainly some correlation between the contours of RMSV and the modelled caustic in the southern Atlantic, some improvements need to be made at the data processing stage to ensure a proper analysis can be carried out. Firstly it is important to make use of all of the available data such that nothing important is missed out from the analysis. It is also important to ensure that the westward propagating signals which we are primarily interested in have been properly isolated. A common technique to extract westward propagating signals from ocean data is the Radon Transform which is used frequently in recent studies, such as Chelton and Schlax (1996). Ensuring that the data is processed correctly is the first step to ensuring an accurate interpretation of the data, and thus also to see if caustics can be identified in real ocean data.

## Chapter 4

# Conclusions and Further Work

### 4.1 Summary

During this project we have modelled ray propagation in the Atlantic and Pacific ocean basins both in cartesian and spherical polar coordinates. We began by considering a straight eastern boundary, both north-south orientated and orientated at some angle  $\alpha$ . We then extended the ideas to account for variable coastline geometry and introduced eastern boundaries representative of the Atlantic and Pacific coastlines.

Introducing a variable coastline required us to introduce a new boundary condition dependent on the angle of the coastline  $\alpha$ . The boundary condition was used to determine the initial values of the zonal and meridional wavenumbers. Having introduced the new boundary condition, it was found that trapped waves in regions equatorwards of the critical latitude  $\phi_c$  were unable to propagate freely as Rossby waves if  $\alpha$  is sufficiently large. This indicates that Rossby waves are not able to propagate from all regions equatorwards of  $\phi_c$ . Variable coastal geometry also creates differences in the initial tilting of the rays as they propagate away from the boundary, and this leads to the divergence and convergence of rays in some regions. The shape of the coastline therefore has significant impacts on the energy distribution of the boundary-driven waves throughout the ocean basin. This observation may be related to the pattern of correlation coefficients shown in Figure (1.2) from Fu and Qiu (2002) and as discussed in Chapter (2.3).

Finally, having previously assumed the phase speed to be constant, we introduced a variable phase speed function to more accurately represent the distribution observed in the real oceans, a result not previously derived. Introducing a variable  $c_0$  meant that  $\phi_c$  becomes a function of  $\alpha$  and  $c_0$ , and the critical coastline angle  $\alpha_c$  becomes a function of  $\phi$  and  $c_0$ . The variable phase speed therefore affects the location of the critical latitude, and

also determines whether Rossby waves can propagate freely from regions equatorwards of  $\phi_c$  if  $\alpha$  is also significant. As the Rossby radius of deformation  $R$  is dependent on  $c_0$  and we determined that the latitudinal variation in  $R$  was significant for shaping the ray envelope, we deduced that  $c_0$  is also an important variable in determining the location of the caustics.

The solutions derived in cartesian coordinates and spherical coordinates were found to be very similar, indicating that the shape of the ray envelope is not strongly dependent on the sphericity of the Earth.

Having produced some graphical representation of the ray propagation patterns across each ocean basin, we briefly discussed the presence of the caustics. The caustics are theoretical lines that meet the eastern boundary at the critical latitude and North of which we expect waves at the boundary to remain trapped as coastally-trapped Kelvin waves. Equatorwards of the critical latitude, provided that the coastline angle is not sufficiently large, waves can propagate freely from the coast as Rossby waves. In the interior ocean, the caustics define the western extent of the region where we expect to find a significant amount of variability associated with boundary driven waves. Westward of the caustic, variability associated with the boundary driven waves is expected to decay exponentially. The pattern of real ray solutions within the caustic region indicated that rays propagating from the eastern boundary turned and headed equatorwards. As a ray trajectory represents the group velocity vector, and energy associated with boundary driven Rossby waves propagates with the group velocity, the theory therefore indicates that energy from the mid-latitudes propagates equatorwards via dispersion, as opposed to the western part of the ocean basin. The turning of the rays, and thus the shape of the ray envelope is what determines the location of the caustics.

Having estimated the location of the caustics in the Atlantic and Pacific oceans, we then aimed to find some correlation between the caustics derived from our model and some modelled ocean data. We considered high resolution SSH data from the French CLIPPER Model in the southern Atlantic Ocean. Due to computational constraints we were limited to the use of 22 zonal sections at  $2.5^\circ$  latitudinal intervals. Initially we carried out some Fourier analysis on the available data and removed the zonal mean in an attempt to isolate the baroclinic Rossby waves. Finally we arranged the data into time-longitude arrays before calculating the RMSV for each zonal section. In plotting contours of the RMSV in the South Atlantic (Figure 3.4), we expected to find greater variance within the region bounded by the caustics estimated from our model. While in some ways the contour plot was somewhat contradictory of our expectations (likely a result of not properly isolating the Rossby wave signal), we still found some correlation between the shape of some of

the contours and the modelled caustic. This is a good early indicator that dispersion is the underlying mechanism resulting in the western decay of baroclinic boundary-driven Rossby waves. If further analysis confirms this result, then it can be deduced that Rossby waves observed in the western part of ocean basins are unlikely to have been generated at the eastern boundary, but produced by an altogether different mechanism.

## 4.2 Further Work

Finally we suggest a number of improvements that can be made to the model itself, and where this work can be taken next.

### 4.2.1 Model Improvements

A latitude-dependent analytical function was introduced to account for the variable Rossby wave phase speeds observed in the real Atlantic and Pacific oceans. While the function used was an improvement on assuming the phase speed to be constant in the ocean overall, it was particularly weak in some parts of the ocean basins. Further to this, an analytical function in latitude and longitude was derived and while not fully implemented, it was shown that it provided a better estimate of the gravity-wave phase speed distribution. Despite this, a good idea would be to use a dataset of observed values of  $c_0$  in conjunction with Matlab's built in two-dimensional interpolation function. This would involve initially assigning the observed values of  $c_0$  onto a discrete array. Then by using spline or nearest interpolation, phase speed values can be taken from the  $c_0(\lambda, \phi)$  array as each ray trajectory is integrated across the ocean basin. When solving the system of ODEs, we must also remember that this will involve a  $c'_0(\lambda, \phi)$  term, making it a little more difficult to implement. This can be solved by including a subroutine called within the ODE function, such that it calculates the rate of change of the observed phase speeds with respect to latitude and longitude. Having deduced that  $c_0$  is an important factor in determining the critical latitude and ray envelope shape, this should be a significant improvement to the model.

A further weakness in the model relates to the determination of the caustics. Whilst we relied on the assumption that the meridional wavenumber  $k_\phi$  along the boundary was zero, the location of the caustic could easily be seen. However, upon introducing a variable  $k_\phi$  along the boundary, the initial points at which the ray trajectories crossed, ie. the points that determine the caustic line, were no longer as easy to see. Determining the caustics therefore became somewhat subjective. It can be assumed that interpolating observed phase speed data is likely to enhance this effect, as an observational dataset is unlikely to be as smoothly varying as the phase speed distribution specified by an analytical formula.

The next step to improve the model is therefore to include some steps to compute the point at which each ray trajectory first crosses with another. The line that passes through each of these points is the caustic.

We previously stated that a caustic appears when two neighboring trajectories, from  $\xi$  and  $\xi + \delta\xi$  (where  $\xi$  is a measure of the distance along the boundary) meet at the same time  $t$ , i.e. when:

$$\begin{aligned}\lambda(t, \xi) &= \lambda(t + \delta t, \xi + \delta\xi) \\ \phi(t, \xi) &= \phi(t + \delta t, \xi + \delta\xi)\end{aligned}\tag{4.1}$$

Expanding the right hand sides yields:

$$\begin{aligned}\delta t \frac{\partial \lambda}{\partial t} + \delta \xi \frac{\partial \lambda}{\partial \xi} &= 0 \\ \delta t \frac{\partial \phi}{\partial t} + \delta \xi \frac{\partial \phi}{\partial \xi} &= 0\end{aligned}\tag{4.2}$$

If we then eliminate the small quantities, it is clear that a caustic occurs when:

$$\frac{\partial \lambda}{\partial t} \frac{\partial \phi}{\partial \xi} - \frac{\partial \phi}{\partial t} \frac{\partial \lambda}{\partial \xi} = 0\tag{4.3}$$

According to Killworth and Blundell (1999), in order to follow the values of this Jacobian, we need differentials of the entire ray problem and the initial conditions with respect to the distance  $\xi$ . As the existing ray problem already consists of derivatives of  $\omega$ , we therefore need to calculate the second derivatives of  $\omega$  with respect to  $\phi$ ,  $\lambda$ ,  $k_\lambda$  and  $k_\phi$ . Calculating the individual points at which a caustic occurs should be sufficient to determine the caustic lines that bound the ray envelope.

Lastly, the model should be extended to examine ray propagation and the presence of caustics in the Indian Ocean. This will simply be a case of altering the array of coastline coordinates to represent the eastern coastline of the Indian Ocean. The array can then be used to determine the initial values of the ray trajectories. A phase speed distribution representative of those in the Indian Ocean should also be used, either through an analytical formula, or through observational data.

### 4.2.2 Ocean Data Analysis

Having made improvements to the ray propagation model, the next stage is to make a full comparison with an oceanic data set, for example from the French CLIPPER model. For this to be successful however, it is important to both utilise all of the available data, but also to ensure that the data is processed correctly. The reason that we wish to process the oceanic data is so that we can isolate the westward propagating Rossby wave signals. Having done so we can recalculate the RMSV in an attempt to locate caustics in the real ocean data.

When considering the SSH anomaly time series in the South Atlantic Ocean, we carried out a Fourier analysis in order to extract the annually varying signal, and removed the zonal averages to ensure that they did not dominate the Rossby wave signals. These methods were not sufficient to extract the Rossby wave signals from the oceanic dataset.

The Radon Transform (Radon, 1917) is a method frequently used in image processing and particularly for extracting information about oceanic Rossby waves. The classical two-dimensional Radon Transform can project an image from the cartesian  $(x, t)$  plane onto a line orientated at a given angle  $\theta$ . The transform effectively calculates the line integral through the  $(x, t)$  image where the line is positioned according to the values of  $\rho$  and  $\theta$  where  $\rho$  is equal to the smallest distance to the origin of the coordinate system. There are various forms of the Radon Transform and some of these have been designed specifically for extracting Rossby wave signals (Lecointre et al. 2008). The following equation represents one form of the Radon Transform:

$$\rho = x \cos \theta + y \sin \theta \quad (4.4)$$

$$R(\rho, \theta) = \int_{-\infty}^{\infty} \int_{-\infty}^{\infty} f(x, y) \delta(\rho - x \cos \theta - y \sin \theta) dx dy \quad (4.5)$$

where  $\rho$  and  $\theta$  are as defined above. Consider the line labelled  $x'$  in Figure (4.1). As this line is rotated through certain angles of  $\theta$ , a line integral is calculated through the image, perpendicular to  $x'$ . By calculating the line integral at certain angles through the image, one can determine the maxima and minima in  $\theta$  corresponding to the image intensity returned from the line integral.

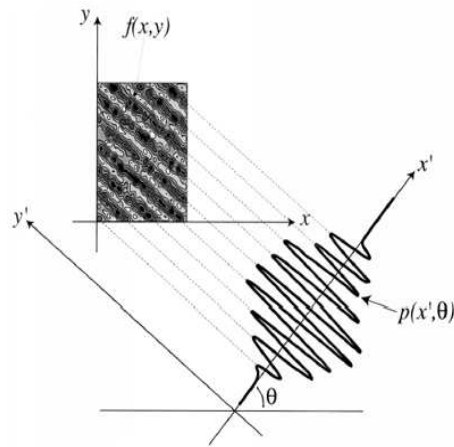


Figure 4.1: Challenor et al. (2001)

As we have seen, westward propagating signals in ocean data can best be illustrated by arranging data into a Hovmöller diagram. Zonally-propagating features subsequently appear as slanted propagation patterns where the angle at which the feature slants is determined by its phase speed. Having applied the Radon Transform to a Hovmöller diagram, we would therefore expect a maxima to occur in  $\theta$  when  $x'$  is perpendicular to the sloping features that represent the westward propagating signals. By determining the maxima and minima associated with certain angles within the time-longitude plot, we can thus identify signals that are purely westward propagating. Then by applying a Gaussian filter, as in Hunt (2009), we can extract the relevant information and apply the Inverse Radon Transform to project the image back onto the  $(x, t)$  plane.

Having calculated the caustics in the ray propagation model numerically and correctly processed the oceanic dataset such that only the annual Rossby wave signal remains, a full quantitative analysis can be performed between the modelled caustics and the Rossby wave SSH variability.

## Chapter 5

# Appendix 1

### 5.1 Variable $c_0$ Equation - Cartesian Coordinates

The analytical phase speed function in  $y$  is defined as:

$$c_0(y) = A + B \cos\left(\frac{2y}{a} + C\pi\right) + D \cos\left(\frac{6y}{a} + \pi\right); \quad (5.1)$$

We need to rederive the equation for the rate of change of  $k_y$  with respect to  $x$ , given by:

$$\frac{dk_y}{dx} = \frac{(R^2)_y k_x}{R^2 [1 + R^2 (k_y^2 - k_x^2)]} \quad (5.2)$$

Thus we simply need to find the derivative of  $R^2$  with respect to  $y$ . First we define:

$$\phi_1 = \frac{6y}{a} + \pi \quad (5.3)$$

$$\phi_2 = \frac{2y}{a} + C\pi \quad (5.4)$$

We will also define:

$$d_1 = \beta^2 y^3 \quad (5.5)$$

$$d_2 = a\beta^2 y^2 \quad (5.6)$$

The following equations are the terms of the resulting derivative of  $R^2$ .

$$r_1 = \frac{2A^2}{d_1} \quad (5.7)$$

$$r_2 = \frac{4AB \sin\phi_2}{d_2} \quad (5.8)$$

$$r_3 = \frac{4AB\cos\phi_2}{d_1} \quad (5.9)$$

$$r_4 = \frac{12AD\sin\phi_1}{d_2} \quad (5.10)$$

$$r_5 = \frac{4AD\cos\phi_1}{d_1} \quad (5.11)$$

$$r_6 = \frac{4B^2\cos\phi_2\sin\phi_2}{d_2} \quad (5.12)$$

$$r_7 = \frac{2B^2\cos^2\phi_2}{d_1} \quad (5.13)$$

$$r_8 = \frac{4BD\cos\phi_2\cos\phi_1}{d_2} \quad (5.14)$$

$$r_9 = \frac{12BD\cos\phi_2\sin\phi_1}{d_2} \quad (5.15)$$

$$r_{10} = \frac{4BD\cos\phi_2\cos\phi_1}{d_1} \quad (5.16)$$

$$r_{11} = \frac{12D^2\sin\phi_1\cos\phi_1}{d_2} \quad (5.17)$$

$$r_{12} = \frac{2D^2\cos^2\phi_1}{d_1} \quad (5.18)$$

Thus we use the following in our equation for  $k_y$ :

$$(R^2)_y = \sum_{i=1}^{12} r_i \quad (5.19)$$

## 5.2 Variable $c_0$ Equation - Spherical Polar Coordinates

The analytical phase speed function in  $\phi$  is defined as:

$$c_0(y) = A + B\cos(2\phi + C\pi) + D\cos(6\phi + \pi); \quad (5.20)$$

We need to re-derive the equation for the rate of change of  $k_\phi$  with respect to  $\lambda$ . Thus we need to determine  $(R^2)_\phi$ . First we define:

$$\phi_1 = 6\phi + \pi \quad (5.21)$$

$$\phi_2 = 2\phi + C\pi \quad (5.22)$$

We also define:

$$(f^2)_\phi = 8\Omega^2 \cos\phi \sin\phi \quad (5.23)$$

The following equations are the terms of the resulting derivative of  $R^2$ :

$$q_1 = \frac{A^2(f^2)_\phi}{f^4} \quad (5.24)$$

$$q_2 = \frac{4AB \sin\phi_2}{f^2} \quad (5.25)$$

$$q_3 = \frac{2AB \cos\phi_2 (f^2)_\phi}{f^4} \quad (5.26)$$

$$q_4 = \frac{12AD \sin\phi_1}{f^2} \quad (5.27)$$

$$q_5 = \frac{2AD \cos\phi_1 (f^2)_\phi}{f^4} \quad (5.28)$$

$$q_6 = \frac{12BD \sin\phi_1 \cos\phi_2}{f^2} \quad (5.29)$$

$$q_7 = \frac{4BD \cos\phi_1 \sin\phi_2}{f^2} \quad (5.30)$$

$$q_8 = \frac{2BD \cos\phi_1 \cos\phi_2 (f^2)_\phi}{f^4} \quad (5.31)$$

$$q_9 = \frac{8B^2 \cos\phi_2 \sin\phi_2}{f^2} \quad (5.32)$$

$$q_{10} = \frac{B^2 \cos^2\phi_2 (f^2)_\phi}{f^4} \quad (5.33)$$

$$q_{11} = \frac{12D^2 \cos\phi_1 \sin\phi_1}{f^2} \quad (5.34)$$

$$q_{12} = \frac{D^2 \cos^2\phi_1 (f^2)_\phi}{f^4} \quad (5.35)$$

Therefore the derivative of  $R^2$  is:

$$(R^2)_\phi = \sum_{i=1}^{12} q_i \quad (5.36)$$

The equation for  $k_\phi$  becomes:

$$\frac{dk_\phi}{d\lambda} = \frac{((R^2)_\phi a^2 \cos^3\phi - 2R^4 \sin\phi k_\lambda^2) k_\lambda}{R^4 \cos^3\phi \left[ a^2 + R^2 \left( k_\phi^2 - k_\lambda^2 / \cos^2\phi \right) \right]} \quad (5.37)$$

## Chapter 6

# References

Challenor, P. G., Cipollini P., Cromwell D., 2001, Use of the 3D Radon Transform to Examine the Properties of Oceanic Rossby Waves, *J. Atmos. Ocn. Tech.*, 18, 1558-1566

Chelton D. B., Schlax M. G., 1996, Global Observations of Oceanic Rossby Waves, *Science*, 272, 234-238

Chelton D. B., DeSzoeki R. A., Schlax M. G., Naggar K., Siwertz N., 1998, Geographical Variability of the First Baroclinic Rossby Radius of Deformation, *J. Phys. Oceanogr.*, 28, 433-460

Fu L.-L., Qiu B., 2002, Low-frequency variability of the North Pacific Ocean: The roles of boundary- and wind-driven baroclinic Rossby waves, *J. Geophys. Res*, 107(C12), 3220, doi:10.1029/2001JC001131

Grimshaw R., Allen J. S., 1983, Low-Frequency Baroclinic Waves off Coastal Boundaries, *J. Phys. Oceanogr.*, 18, 1124-1142

Hunt F., 2009, The Vertical Structure of Oceanic Rossby Waves, *University of Reading MSc Dissertation*

Killworth, P. D., Chelton D. B., de Szoeki R. A., 1997, The speed of observed and theoretical long extratropical planetary waves, *J. Phys. Oceanogr.*, 27, 1946-1966

Killworth P. D., Blundell J. R., 1999, The Effect of Bottom Topography on the Speed of Long Extratropical Planetary Waves, *J. Phys. Oceanogr.*, 29, 2689-2710

- Killworth P. D., Blundell J. R., 2003, The Dispersion Relation for Planetary Waves in the Presence of Mean Flow and Topography. Part I: Analytical Theory and One-Dimensional Examples, *J. Phys. Oceanogr.*, 34, 2692-2711
- LeBlond P. H., Mysak L. A., 1978, Waves in the Ocean, *Elsevier Scientific Publishing Company*
- Lecointre A. et al., 2008, Depth Dependence of Westward Propagating North Atlantic Features Diagnosed from Altimetry and a Numerical 1/6 Degree Model, *Ocean Science*, 4, pp.99-113
- Pedloski J., 1986, Geophysical Fluid Dynamics Second Edition, *Springer*
- Pedloski J., 2003, Waves in the Ocean and Atmosphere - Introduction to Wave Dynamics, *Springer*
- Radon J., 1917, Uber die Bestimmung von Funktionen durch ihre Integralwerte langs Gewisser Mannigfaltigkeiten, *Berichte Sachsische Akademie der Wissenschaften, Leipzig. Math.-Phys.*, 69, pp.262-67.
- Rossby C. -G., 1939, Relation Between Variations in the Intensity of the Zonal Circulation of the Atmosphere and the Displacements of the Semi-permanent Centers of Action, *J. Mar. Res.*, Vol. II, No. 1, 38-55
- Schopf P. S., Anderson D. L. T., Smith R., 1981, Beta-Dispersion of Low-Frequency Rossby Waves, *Dyn. Atmos. Oceans*, 5, 187-214
- Tailleux R., McWilliams J. C., 2002, Energy Propagation of Long Extratropical Rossby Waves Over Slowly Varying Zonal Topography, *J. Fluid Mech.*, 473, 295-319
- Treguier A. M. et al., 1999, The CLIPPER Project: High Resolution Modelling of the Atlantic. *International WOCE Newsletter*, 36, pp.3-5